THE BRAZIL CURRENT AND INTERMEDIATE WESTERN BOUNDARY CURRENT FLOWS THROUGH THE VITÓRIA-TRINDADE RIDGE

Fernando Dix Terra Barberini

Dissertação de Mestrado apresentada ao Programa de Pós-graduação em Engenharia Oceânica, COPPE, da Universidade Federal do Rio de Janeiro, como parte dos requisitos necessários à obtenção do título de Mestre em Engenharia Oceânica.

Orientador: Afonso de Moraes Paiva

Rio de Janeiro
Outubro de 2017

THE BRAZIL CURRENT AND INTERMEDIATE WESTERN BOUNDARY CURRENT FLOWS THROUGH THE VITÓRIA-TRINDADE RIDGE

Fernando Dix Terra Barberini

DISSERTAÇÃO SUBMETIDA AO CORPO DOCENTE DO INSTITUTO ALBERTO LUIZ COIMBRA DE PÓS-GRADUAÇÃO E PESQUISA DE ENGENHARIA (COPPE) DA UNIVERSIDADE FEDERAL DO RIO DE JANEIRO COMO PARTE DOS REQUISITOS NECESSÁRIOS PARA A OBTENÇÃO DO GRAU DE MESTRE EM CIÊNCIAS EM ENGENHARIA OCEÂNICA.

Examinada por:

_____
Prof. Afonso de Moraes Paiva, Ph.D.

_____
Prof. Mauro Cirano, Ph.D.

_____
Prof. Marcos Nicolás Gallo, D.Sc.

RIO DE JANEIRO, RJ - BRASIL
OUTUBRO DE 2017

Barberini, Fernando Dix Terra

The Brazil Current and Intermediate Western Boundary Current flows through the Vitória-Trindade ridge/Fernando Dix Terra Barberini. – Rio de Janeiro: UFRJ/COPPE, 2017.

XIII, 73 p.: il.; 29,7 cm.

Orientador: Afonso de Moraes Paiva

Dissertação (mestrado) – UFRJ/ COPPE/ Programa de Engenharia Oceânica, 2017.

Referências Bibliográficas: p. 40-46.

1. Brazil Current. 2. Intermediate Western Boundary Current. 3. Vitória-Trindade ridge. I. Paiva, Afonso de Moraes. II. Universidade Federal do Rio de Janeiro, COPPE, Programa de Engenharia Oceânica. III. Título.

Knowledge comes from learning. Wisdom comes from living.

Anthony Douglas Williams

Acknowledgements

First, I thank God for giving me strength and guidance in this important phase of my life that has just been completed. I thank my parents and all my family, who have always been by my side, supporting me and encouraging all my life decisions. I thank my advisor Afonso Paiva for guiding me during these years and for providing me incredible learning opportunities. I thank Professor Mauro Cirano for the opportunity of working with him at SiMCosta since 2016, and all my friends from the Laboratory of Physical Oceanography (LOF-COPPE) for their companionship and productive discussions, especially Vladimir and Guilherme. I thank all the amazing professors from the Ocean Engineering Program at COPPE-UFRJ, who have contributed to my academic growth: Marcos Nicolas Gallo, Afonso Paiva, Carlos Parente, Paulo Cesar Colonna Rosman, Nelson Violante, Susana Vinzon, Jean David, and Severino Fonseca da Silva Neto. Also, I acknowledge the Brazilian Navy for providing the oceanographic data used in this work.

Financial support for this work was provided by the Coordenação de Aperfeiçoamento de Pessoal de Nível Superior (CAPES) Foundation.

Resumo da Dissertação apresentada à COPPE/UFRJ como parte dos requisitos necessários para a obtenção do grau de Mestre em Ciências (M.Sc.)

FLUXOS DA CORRENTE DO BRASIL E DA CORRENTE DE CONTORNO INTERMEDIÁRIA ATRAVÉS DA CADEIA VITÓRIA-TRINDADE

Fernando Dix Terra Barberini

Outubro/2017

Orientador: Afonso de Moraes Paiva

Programa: Engenharia Oceânica

Com o objetivo de contribuir para a descrição dos fluxos da Corrente do Brasil (CB) e da Corrente de Contorno Intermediária (CCI) através da Cadeia Vitória-Trindade (CVT), este trabalho compila dados de três comissões oceanográficas realizadas em 2013 e 2014 entre 19 e 23°S. Uma das comissões foi especialmente desenhada para o estudo dos fluxos nas principais passagens entre os montes da CVT e as outras duas foram levantamentos oceanográficos sistemáticos realizados pela Marinha do Brasil na região. O estudo analisa um total de 83 estações oceanográficas e dados de ADCP de casco. Uma análise conjunta de dados de sensoriamento remoto foi realizada em feições de mesoescala que foram amostradas durante os cruzeiros. A CB sofreu um processo de intensificação com o aumento da latitude. Na região dos montes submersos, núcleos da CB foram observados entre o Banco de Abrolhos e o Banco Besnard, entre o Banco Besnard e o Monte Vitória e ao sul do Monte Vitória. A zona entre ~20 e ~21,5 °S apresentou-se como uma região de reorganização da CB junto ao talude continental e ao sul de 21,5°S, o fluxo apresentou-se com grande intensidade. A CCI também foi intensificada ao longo de sua trajetória para o norte. O fluxo da corrente foi observado em três caminhos preferenciais entre os montes da CVT. No canal entre o Banco Besnard e Monte Vitória, o maior volume de transporte pôde ser observado. A importância da ACAS e AIA no fluxo da CCI foi comparável entre 19 e 22 °S. Em 19,5 °S pôde-se verificar a CCI organizada em um ramo único e intenso. Vórtices ciclônicos e anti-ciclônicos, amostrados durante os cruzeiros, atingiram profundidades superiores a 500m, influenciando assim a circulação tanto a CB como da CCI.

Abstract of Dissertation presented to COPPE/UFRJ as a partial fulfillment of the requirements for the degree of Master of Science (M.Sc.)

THE BRAZIL CURRENT AND INTERMEDIATE WESTERN BOUNDARY CURRENT FLOWS THROUGH THE VITÓRIA-TRINDADE RIDGE

Fernando Dix Terra Barberini

October/2017

Advisor: Afonso de Moraes Paiva

Department: Ocean Engineering

In order to contribute to the description of the flows of the Brazil Current (BC) and the Intermediate Western Boundary Current (IWBC) through the submerged seamounts of the Vitória-Trindade Ridge (VTR), this work compiles data from three oceanographic commissions that took place in 2013 and 2014, between 19 e 23°S. One of the commissions was specially designed for the study of the flows in the main passages between the CVT seamounts, and the other two were systematic oceanographic surveys conducted by the Brazilian Navy in the region. The study analyzes a total of 83 oceanographic stations and vessel-mounted ADCP measurements. A combined analysis of remote sensing data was performed on mesoscale features that were sampled during the cruises. As the latitude increased, the BC was intensified. In the region of the seamounts, BC cores were observed between the Abrolhos Bank and the Besnard Bank, between the Besnard Bank and Vitória Seamount, and to the south of the Vitória Seamount. The zone between ~ 20 and ~ 21.5 ° S was characterized as a region where the BC flow got reorganized by the continental slope. To the south of 21,5 ° S, the flow presented high intensity. The IWBC was also intensified along its trajectory towards north. The flow was divided into three paths at the seamounts region. Through the channel between the Besnard Bank and Monte Vitória, the greater volume transport was observed. The importance of SACW and AAIW in the IWBC flow was comparable between 22 and 19 °S. At 19.5 ° S it was possible to verify that the IWBC was organized as a single and intense branch. Cyclonic and anti-cyclonic eddies, which were sampled during the cruises, reached depths greater than 500m, thus influencing the circulation of the BC and IWBC in the region.

Contents

List of Figures

List of Tables

List of Acronyms

AAIW – Antartic Intermediate Water

AVISO - Archiving Validation and Interpretation of Satelite Data in Oceanography

BC – Brazil Current

Chla – Chlorophyll-a

CODAS - Common Ocean Data Access System

CTD – Conductivity - Temperature – Depth

DWBC – Deep Western Boundary Current

GPS - Global Positioning System

IWBC – Intermediate Western Boundary Current

LADCP – Lowered Acoustic Doppler Current Profiler

LTA - Long Term Averages

MOC – Meridional Overturning Circulation

MODIS - Moderate Resolution Imaging Spectroradiometer

MSLA – Mean Sea Level Anomaly

NADW – North Atlantic Deep Water

NBUC – North Brazil Undercurrent

OSTIA - Operational Sea Surface Temperature and Sea Ice Analysis

SACW – South Atlantic Central Water

SASG South Atlantic Subtropical Gyre

SEC – South Equatorial Current

SST – Sea Surface Temperature

UCPW - Upper Circumpolar Water

VMADCP – Vessel Mounted Acoustic Doppler Current Profiler

VTR – Vitória-Trindade Ridge

WBC – Western Boundary Current

Opening Remarks

This work contains four chapters and three appendix sections. The four chapters (introduction, methods, results, and discussion and conclusion) are an article-like section that aims to characterize the Brazil Current and Intermediate Western Boundary Current in the Vitória-Trindade Ridge region, and how these two currents negotiate their way to get through the physical barrier imposed by the seamounts. The description of the currents is focused between the latitudes of 19ºS and 23ºS. Mesoscale features that were sampled during the oceanographic cruises are also reported. Additional informations and details related to the research that did not fit into this article-like section are presented in the appendix sections. Appendix A presents a general introduction to the ocean circulation off the Brazilian coast, Appendix B describes the data processing procedures, and Appendix C presents all vertical sections of ADCP (Acoustic Doppler Current Profiler) and geostrophic velocity that were analyzed in this work.

Chapter 1
Introduction

The Western Boundary Currents (WBCs) play a key role in the transport of water properties along the Brazilian coast. This system of deep and surface currents is of great importance for the distribution of water masses, and consequently, heat, salt, carbon, and nutrients. Between the latitudes of 15ºS and 25ºS, the WBCs are characterized by a complex depth-dependent pattern composed by the Brazil Current (BC), Intermediate Western Boundary Current (IWBC), and Deep Western Boundary Current (DWBC) (Stramma and England, 1999). On the top layer, the BC flows southward, and its trajectory is highly influenced by mesoscale features (Schmid et al., 1995; Soutelino et al., 2011; Mill et al., 2015). Such interactions are also observed in the intermediate layer (Legeais et al., 2013; Mill et al., 2015; Costa et al., 2017), where the IWBC flows northward, and in the DWBC (Garzoli et al., 2015).

At 20 ºS, the Vitória-Trindade Ridge (VTR) constitute a major topographic barrier for the WBCs in the South Atlantic. Morphologically, the VTR is formed by zonally disposed seamounts that extend eastward from the continental shelf to ~ 29 °W, in the latitude range of 19.5ºS – 21ºS. The Trindade and Martin Vaz islands represent the eastern limit of the ridge and also the only two emerged seamounts. The other seamounts are submerged, and they can reach tens of meters from the ocean surface. Thus, whenever the ocean currents reach the VTR, the flows have to work out their way through the narrow channels created by the bottom topography (Evans et al., 1983; Evans and Signorini, 1985; Boebel et al., 1999; Legeais et al., 2013; Costa et al.,2017).

Since not many studies have been done at the region to describe the ocean circulation, there are several uncertainties about the BC and IWBC behavior whenever they reach this complex bathymetry. Evans et al. (1983) were the first to partially describe the CB flow at ~20 ºS. After analyzing hydrographic data between 19 ºS and 22 ºS, the authors concluded that most of the BC flow crosses the VTR region through the channel between the Besnard Bank and the Vitória Seamount (Figure 1.1), with maximum velocity of 52 cm/s and transports of 3.8 Sv (500 m) (1Sv = 10^6 m^3/s) and 6.8 Sv (1000 m). However, the presence of the BC and its transport in other channels had never been investigated before Evans and Signorini (1985). Evans and Signorini (1985) made current measurements not only in the channel between the Besnard Bank and Vitória Seamount, but also between the Vitória and Montague seamounts. The surface flows in these two stations were southward, evidencing the presence of the BC in both channels. A northward flow of the IWBC was also present in deeper layers at these locations. Thus, the flux division of the two currents due to the physical barrier imposed by the VTR became evident.

Lagrangian observations and long current meter records have also pointed to the division of the IWBC flow at the seamounts region (Muller et al., 1998; Legeais et al., 2013; Costa et al., 2017). Boebel et al. (1999), who observed drifter trajectories at the intermediate depth, described the current as quasi-continuous from 28 ºS to 2 ºS. The mean speed was ~30 cm/s, and the northward transport was of 4 ±2 Sv. Particularly at the VTR region, Legeais et al. (2013) looked into routes of RAFOS-type floats drifting at 800 m deep, between 1994 and 2003, and verified that the IWBC uses at least two paths on its way north. From the total of 11 float trajectories that were analyzed, 9 pointed to an IWBC route through the channel between the Besnard Bank and the

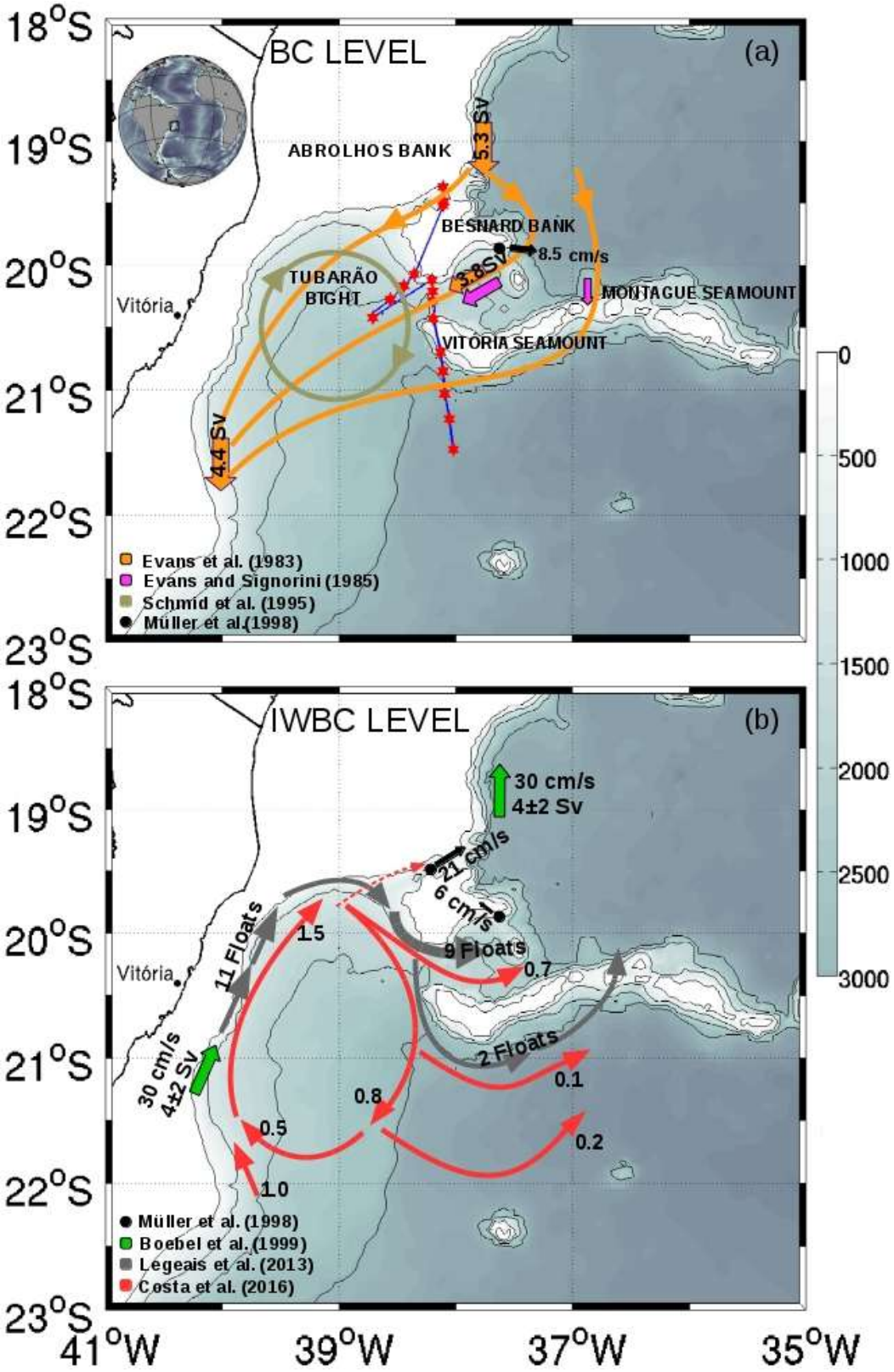

Figure 1.1: Circulation scheme at the (a) BC and (b) IWBC levels, according to studies available in literature. Red hexagons indicate the locations of hydrographic stations during the VTR-Fluxes cruise (data set used in this study - August/2014), while the blue line represents the vessel route. Black circles, related to Muller et al. (1998) study, indicate the mooring locations.

Vitória Seamounts after turning clockwise inside the Tubarão Bight (Figure 1.1). Two other floats also followed the continental slope inside the bight before reaching the VTR. However, instead of turning east in the passage between the Besnard Bank and the Vitória Seamount, the floats passed the southern flank of the Vitória Seamount and crossed the VTR between the Vitória and Montague Seamounts.

In respect to the IWBC routes, the results obtained by Legeais et al. (2013) agreed well with measurements made by Evans and Signorini (1985) and the findings of Costa et al. (2017), since all the studies pointed to the presence of the current in the two paths previously mentioned. However, in terms of preferential routes and direction of the IWBC, the findings of Legeais et al. (2013) and Costa et al. (2017) contradicted the only long current meter record at the region (Muller et al., 1998). Legeais et al.(2013) and Costa et al. (2017) described that the main route of the current was through the channel between Besnard Bank and the Vitória Seamount. In addition, Costa et al. (2017) reported that approximatelly 70% of the IWBC flow uses this path to cross the VTR. On the other hand, Muller et al. (1998) showed that at ~700-800m deep, the current flow was dominant through the channel between the Abrolhos and Besnard banks. According to Muller et al. (1998), the IWBC velocities in this passage were more intense, reaching a mean speed of ~20 cm/s, against only ~6 cm/s in the passage referred by Legeais et al. (2013) and Costa et al. (2017) as the main route of the current.

As a broad picture, articles describing the flows of the BC and IWBC at the VTR region mention three main routes used by these two currents to manage the crossing of the seamounts. However, there has never been an appropriate sampling design to investigate the flows of the two ocean currents through these three passages. Moreover, most ocean circulation studies in this area are based on geostrophic calculations only,

which are associate to some level of uncertainty due to the definition of the level of no motion.

Thus, in order to reach an ocean circulation scenario as close as possible to reality, this work aims to characterize the BC and IWBC flows in the vicinity of the VTR. The volume transports, velocities, and vertical structures are described, as well as the water masses transported by these two currents. A special sampling design was created to measure the BC and IWBC in the three main passages of the VTR region, and a Lowered Acoustic Doppler Current Profiler (LADCP) was used at the oceanographic stations. In addition, data sets from two other complementary oceanographic cruises performed between the latitudes of 19 ºS and 23 ºS provided support for the description of the flows in the area. All the three cruises were conducted during 2013 and 2014. Mesoscale features that were occasionally capture during the cruises are also described. In addition, remote sensing data such as Chlorophyll-a (Chla), Sea Surface Temperature (SST), and Mean Sea Level Anomaly (MSLA) provided tools for the identification and description of the features.

Chapter 2

Data and Methods

2.1 Data set

The data set used in this work was acquired during three oceanographic surveys in the context of the [1]PNBOIA III (July 18 – August 15/2013), PNBOIA I (March 8 – April 2/2014), and VTR-FLUXES (August 14 - 16/2014) Projects, aboard NOc *Cruzeiro do Sul* - Brazilian Navy (Figure 2.1). Current measurements were taken continuously along the vessel route by a Vessel-mounted Acoustic Doppler Current Profiler (VMADCP), from RD Instruments. The VMADCP frequency of 75 kHz made possible the record of ocean current information from 35 m to approximately 300 m deep. At the stations, conductivity–temperature–depth (CTD - *Sea-Bird SBE 9*) profiling and LADCP records were made from the surface down to approximately 100m above the oceanic bottom. The LADCP data was recorded during the PNBOIA I and VTR-FLUXES cruises by two 300 kHz Workhorse Sentinel devices (RD Instruments), and the data from the upward-looking and downward-looking devices were later combined during data processing.

A combination of Chla, SST, and MSLA data contributed to the understanding of mesoscale features from a zoomed out perspective. The Chla data is a 8-day composition of a level-3 binned product, which is freely available (http://oceancolor.gsfc.nasa.gov). The use of several days composite is important to minimize the effects of cloud coverage on data acquisition. The data was obtained by the Moderate Resolution Imaging Spectro-

1. The PNBOIA roman numbers identify different cruises within each year.

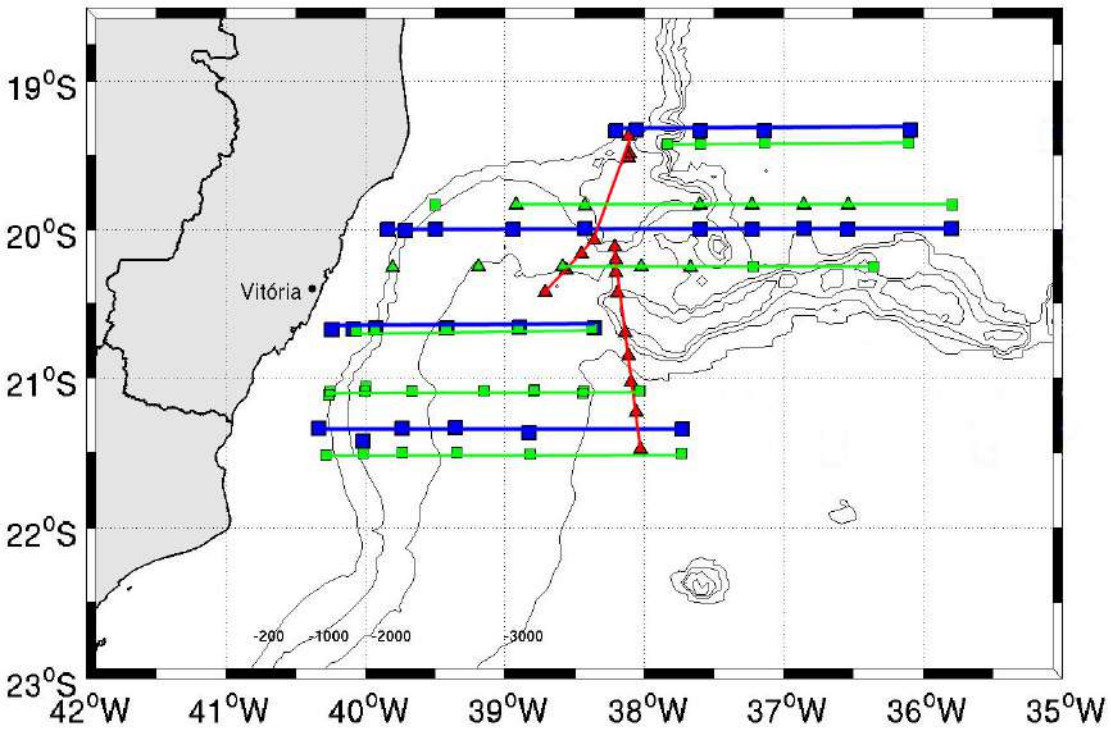

Figure 2.1. Hydrographic stations (markers) and vessels routes (lines) during each of the three research cruises - PNBOIA III (blue), PNBOIA I (green), and VTR-FLUXES (red). Triangles represent LADCP/CTD stations, and squares represent CTD only stations.

radiometer (MODIS) sensor, aboard the Aqua satellite, and had spatial resolution of approximately 4 km. The SST data is from the Operational Sea Surface Temperature and Sea Ice Analysis (OSTIA) 7 days averaged product (Donlon et al., 2012) with resolution close to 5 km. In addition to satellite data provided by the Group for High Resolution Sea Surface Temperature (GHRSST), the OSTIA product also used *in situ* observations to determine the SST. An optimal interpolation, described by Martin et al. (2007), combined the two data types. For MSLA, daily products, produced by SSALTO/DUAVTR-FLUXES and distributed by Archiving Validation and Interpretation of Satelite Data in Oceanography (AVISO – http://www.aviso.oceanobs.com), were used. The MSLA 1/4° x 1/4° gridded products result from an interpolation of multiple along track satellites observations (Le Traon et al., 2003).

2.2 Data processing

A standard SBE Data Processing program (version 7.22.2) was used in order to process the CTD data. For the VMADCP data, the processing was achieved through the Common Ocean Data Access System (CODAS) software, from the Currents Group of the University of Hawaii. After the VMADCP data was processed, it was used during the LADCP data processing. The inverse method procedure that was used to process the LADCP data was based on a set of linear equations (Visbeck, 2002), and the equations took into account not only the VMADCP data, but also the CTD, bottom track, and Global Positioning System (GPS) information to profile the ocean velocities. The VMADCP data was also used to adjust the geostrophic currents. Absolute velocities were obtained by adjusting geostrophic relative velocities to the VMADCP data through the least square fit. Additional data processing details are presented in Appendix B.

Chapter 3
Results

The results are organized as it follows: The BC flow sub-section describes the upper flow velocities and the volume transport in oceanographic sections between 19 and 23 °S. Results are based on VMADCP and LADCP data. The IWBC flow sub-section identifies the water masses volume transported by the IWBC, and also the current velocities in the geostrophic and LADCP sections between 19 and 22 °S. The BC and IWBC vertical sections are presented in the appendix section (Appendix C – C.1 and C.2). Three eddies that were sampled during the oceanographic cruises are described in the Mesoscale Activity item, where physical and biological features of the eddies are discussed.

3.1 The Brazil Current Flow

Based on the VTR-FLUXES VMADCP data, Figure 3.1 presents the upper BC circulation through the seamounts. Arrows indicate the average direction and intensity of ocean currents in the top 100 m, along the vessel's track. According to the data, the BC was flowing westward in the channels between the Abrolhos and Besnard Banks (Figure 3.1- section 1), between the Besnard Bank and Vitória Seamount (Figure 3.1- section 2), and to the south of the Vitória Seamount (Figure 3.1- section 3). Also, the current was observed over the Besnard Bank and Vitória Seamount. Over the latter, the surface current followed the westward dominant flow. However, over the Besnard Bank,

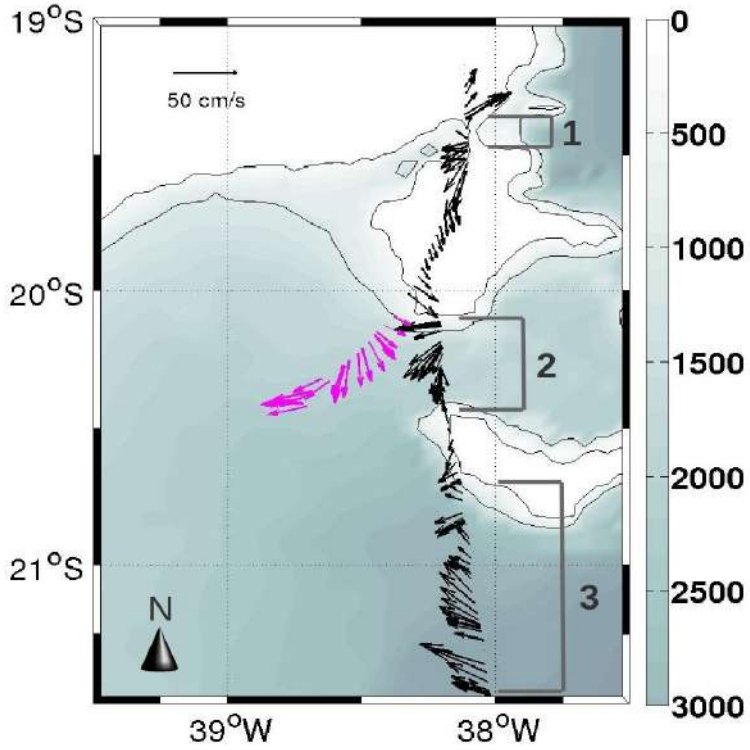

Figure 3.1: Average direction and intensity of ocean currents in the top 100 m during the VTR-FLUXES cruise (August/2014).

the current followed predominately southward, and was being influenced by a recirculation pattern at the Tubarão Bight (Figure 3.1 - pink arrows). This pattern was observed due to the presence of an eddy in the area, and the eddy features will be discussed later (item 3.3), where mesoscale activities are described.

In the northern-most channel (Figure 3.1- section 1), the maximum and mean speeds were 34 cm/s and 10 cm/s, respectively, and the volume transport for the upper 300m was 0.1 Sv. A higher transport was found in the channel between the Besnard Bank and the Vitória Seamount (Figure 3.1- section 2), and an even higher for the flow to the south of the Vitória Seamount (Figure 3.1- section 2). While the central channel volume transport was of 0.2 Sv, with maximum speed of 25 cm/s and mean speed of 9 cm/s, the southern-most flow had 1.2 Sv of transport, maximum speed of 19 cm/s and mean speed of 5 cm/s.

A vertical section of the zonal velocities that were measured during the VTR-FLUXES cruise show more features of the BC between 19.3 and 21.5 °S (Figure 3.2). At the hydrographic stations, the LADCP recorded the flow velocities down to deeper layers in the water column where the VMADCP could not reach. The BC was noticeable from 19.5 to 21.5 °S, with negative surface zonal velocities, and two surface cores were observed. A 20 cm/s core was centered at ~20 °S, and a 10 cm/s ranged from 20.8 to 21.5 °S, where the southernmost current measurement was taken. In the channel between the Abrolhos Bank and the Besnard Bank (~ 19.5 °S), a 10 cm/s subsurface core was observed. This flow spread south over the Besnard Bank and joined the 20 cm/s surface core in the central channel. A westward flow was also noticed over the Vitória Seamount (~ 20.6 °S). Thus, the BC was not limited by the seamounts, but the flow was deeper to the south of the Vitória Seamount. In this portion, the BC reached approximately 500m deep, while to the north of the seamount, the BC maximum depth was 120 – 150 m.

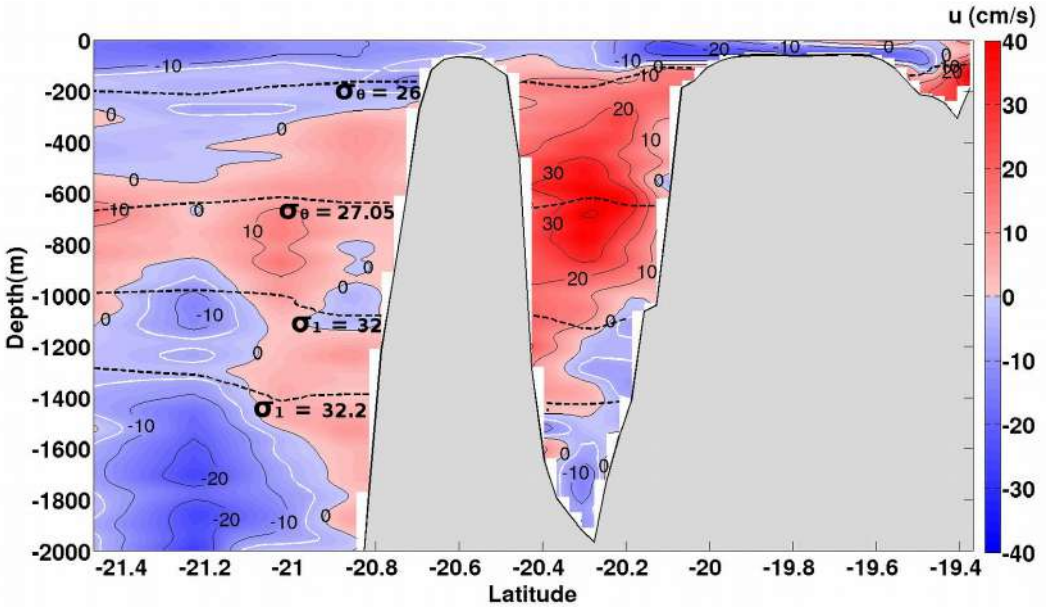

Figura 3.2: Vertical section of zonal velocities measured with LADCP and VMADCP (optimal interpolation) during the VTR-FLUXES cruise in August/2014. Water masses are limited by dashed lines: Tropical Water ($\sigma_\theta < 26$), SACW ($26 < \sigma_\theta < 27.05$), AAIW ($27.05 < \sigma_0$ and $\sigma_1 < 32$), and Upper Circumpolar Water (UCPW $32 < \sigma_1 < 32.2$).

In order to calculate de BC volume transports, this work used VMADCP data from the three cruises (Table 3.1). Between the latitudes of 19°S and 23°S, sections in the continental shelf/slope and in the seamounts regions were selected (Figure 3.3 -S1 to S16). The sections length varied according to the spreading of the BC flow along the vessel's track. Only in the case of sections between seamounts (S14 and S15), the lengths were limited by the widths of the channels.

Table 3.1: Volume transport across each of the sixteen VMADCP sections that captured the BC. Each color represent a different cruise: PNBOIA III (blue), PNBOIA I (red), and Cruzeiro do Sul (green). * indicate that the section had a considerable blank area. Figure 3.3 presents the location of each section, and Appendix C shows the vertical sections not presented in sub-section 3.1.

Section Number	Latitude (°S)	Longitude (°W)	Transport (Sv)	Month/Year	Depth Range (m)
S1	19.35	38.1 - 37.1	-0.8	Aug/2013	35 - 200
S2	19.4	37.9 - 37.2	-1.0	Mar/2014	35 - 100
S3	19.85	38.7 - 36.9	-1.4	Mar/2014	35 - 150*
S4	20	39.7 - 39.1	-1.0	Aug/2013	35 - 150
S5	20	37.9 - 37.3	-0.8	Aug/2013	35 - 200*
S6	20.25	38.1 - 36.6	-0.9	Mar/2014	35 - 160*
S7	20.67	39.9 - 39.45	-2.2	Jul/2013	35 - 300
S8	21.1	40.25 - 39.3	-2.2	Mar/2014	35 - 150
S9	21.1	40.25 - 38.7	-1.4	Feb-Mar/2014	35 - 100
S10	21.3	39.9 - 38.9	-1.5	Jul/2013	35 - 200
S11	21.5	40.2 - 39.5	-1.3	Mar-Apr/2014	35 - 150
S12	22	40.06 - 39.2	-3.7	Aug/2014	35 - 300
S13	23	40.83 - 39.9	-1.7	Feb-Mar/2014	35 - 120*
S14	19.5 - 19.4	38.1	-0.1	Aug/2014	35 - 300
S15	20.57 - 20.05	38.2	-0.2	Aug/2014	35 - 300
S16	21.57 - 20.57	38.1	-1.2	Aug/2014	35 – 300

Before reaching the VTR region, at ~19.4 ºS, the BC volume transport was 0.8 Sv (S1 – Table 3.1; Figure 3.3) in August/2013 and 1.0 Sv (S2 – Table 3.1; Figure 3.3) in March/2014. Even though the volume numbers were close, the current was stronger in

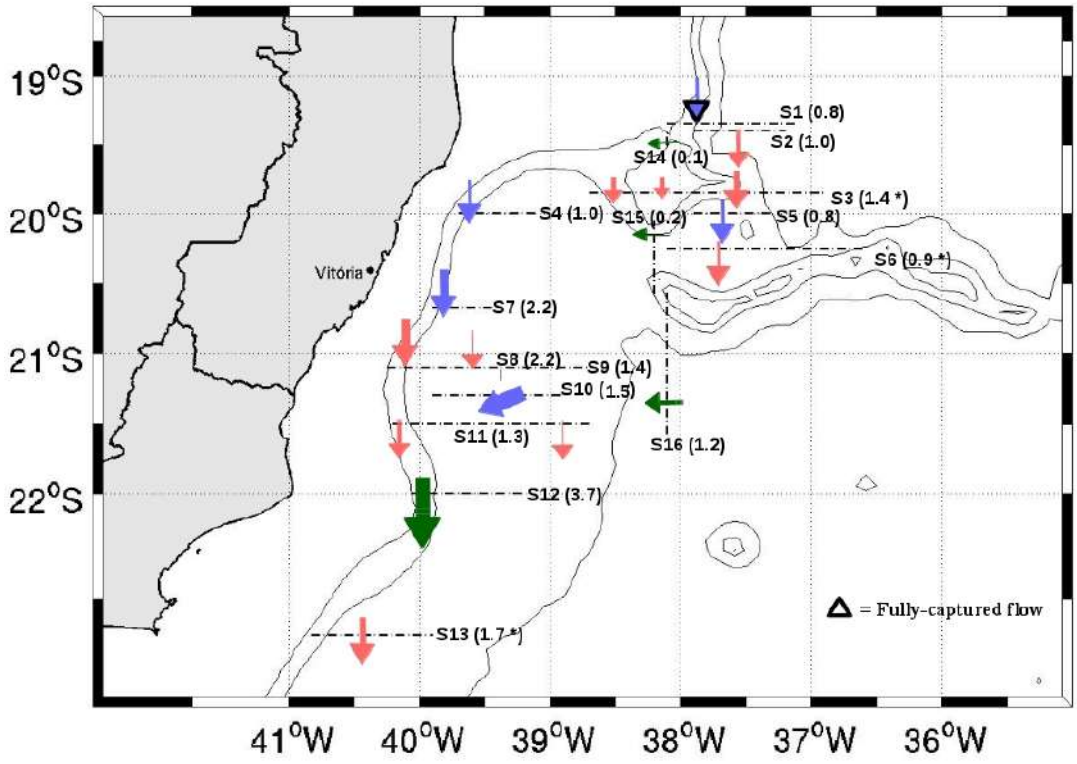

Figure 3.3: Sections (S1 to S16) where the BC flows were calculated from VMADCP measurements. The arrows thickness are proportional to the BC volume, and the arrows positions indicate the BC core (The S10 arrow indicate the dominant direction of the current in the section). Each color represent a different cruise: PNBOIA III (blue), PNBOIA I (red), and VTR-FLUXES (green). The number between parentheses represent the net volume transport in Sv (1 Sv = 10^6 m^3 s^{-1}) (* - indicate that the section had a considerable blank area).

2014. During this year, a smaller water column area was sampled, the BC flow was not fully captured by the measurements, and the meridional velocities were higher. A wide 40 cm/s core was observed, while in 2013 the velocities reached only 32 cm/s. Also, in 2014 the flow core was positioned farther east (S2 – Figure 3.3) than in 2013 (S1 – Figure 3.3).

In the VTR region, during the VTR-FLUXES cruise, the greater part of the current flowed through the channels (S14 and S15 – Figure 3.3) and to the south of the Vitória Seamount (S16 – Figure 3.3), but part of the flow also crossed the region over the Besnard Bank and Vitória Seamount. During the PNBOIA I cruise, from the total of 1.4

Sv at 19.85 °S (S3 – Figure 3.3), 0.1 Sv was transported by the BC over the Besnard Bank, 1.1 Sv to the east of the bank, and 0.2 Sv to the west. The 50 cm/s flow core on the east side (S3 – Figure 3.3) was located at the same longitude as the core at 19.4 °S (S2 – Figure 3.3), between 95 and 120 m deep. To the west of the bank, two cores were observed. Both of them presented the velocity of 30 cm/s, at different depths. One of them, at 38.4º W, was on the surface, while the other was between the depths of 80 and 90 m, at 38.5º W.

Subsurface cores represented a recurrent BC feature that was observed in many sections. At 20 °S, to the east of the Besnard Bank (S5 – Figure 3.3), this feature was also observed. Between 37.5 and 37.75º W, the current had its highest intensity (30 cm/s core) between 130 and 200 m deep. Although an important part of the flow was not measured by the VMADCP, a volume transport of 0.8 Sv was observed.

To the south, at 20.25 °S, the main flow was between 37.2 and 38.1º W (S6 – Figure 3.3). The BC maximum velocities, within the 30 cm/s core, ranged from 37.3 to 37.8º W, in the upper 90 m water column. The volume transport was 0.9 Sv. However, the BC flow at this latitude was not fully captured. In the main flow, the current was measured only down to 100 m. At this depth, the velocities were over 20 cm/s. Consequently, the flow volume transport was expected to be higher.

After the BC crossed the seamounts region, its flow was captured at different latitudinal locations along the continental slope (S4, S7-S13 – Figure 3.3). At 20 °S (S4 – Figure 3.3), the current was organized as an unique branch. The BC volume transport was 1.0 Sv (35 – 150 m), and the region near the slope had the highest velocities. The top 65 m of the water column had velocities higher than 50 cm/s, and according to the measurements, the current reached the depth of 140 m. Further south, at ~20.7 °S (S7 –

Figure 3.3), the flow was diffuse and exhibited two cores. The surface core, at ~39.7 °W was of 20 cm/s, and nearly underneath this core, a 40 cm/s subsurface core was noticed between the depths of 70 and 200 m. The total volume transport was 2.2 Sv (35-300 m).

The same volume transport was found at 21.1 °S (S8 – Figure 3.3). However, the measurements at this latitude were made in 2014. Also, the BC flow area that was considered in the transport calculation was smaller than the area at ~20.7 °S (S7 – Figure 3.3), which suggests again a more intense current during March/2014 than in August/2013. The current velocities at 21.1 °S were also more intense and reached 60 cm/s.

A second BC measurement at 21.1 °S (S9 - Figure 3.3), which was made few days before the vessel cruised S8, revealed changes in the current structure. In this occasion (S9 transect - Figure 3.3), the BC presented two cores with lower intensities (arrows on the S9 line – Figure 3.3). The westernmost core was located at the slope region (as in S8), however the maximum speed was only 43 cm/s. In the second core, between 39.3 and 39.8º W, the velocities were even lower, and the maximum speed was 38 cm/s. The total volume transport was 1.4 Sv. Even though the volume transport in S9 was lower than in S8, the depth considered for calculations was also lower.

In July-August/2013, part of the BC was observed heading southwestward at 21.3 S° (S10 – Figure 3.3). A transport of 1.5 Sv was calculated, and a 30 cm/s core, centered at 39.25º W, was noticed between the depths of 130 and 200 m. This southwestward flow pointed to a BC organization process between 21 and 22ºS. The BC portion that crossed the VRT region through the paths among the seamounts was possibly heading towards the continental slope to adjust the potential vorticity.

At 21.5º S the BC still presented a split flow, but further south, the flow got

organized by the continental shelf break. Similarly to what was observed at 21.1 ºS (S9 – Figure 3.3), at 21.5 °S (S11 – Figure 3.3) the BC also had two cores. One of them nearby the slope area, with higher current velocities, and the other more to the east. While the first reached 60 cm/s, the one on the east side of the section reached only half of that, and the total volume transport was 1.3 Sv (35-150 m). At 22º S, the flow was organized as an unique branch (S12 – Figure 3.3), and this same organization was observed further south (S13 – Figure 3.3). The maximum meridional velocity at 22°S was 74 cm/s, and the current transported 3.7 Sv (35-300 m). The BC had it highest velocity near the ocean's surface. However, elevated velocities could be noticed down to deeper regions. A 40 cm/s core between 220 and 260 m deep was also observed underneath the surface flow, at 39.8º W. At 23 °S (S13 – Figure 3.3), the maximum velocity was 70 cm/s, and the 60 cm/s flow core, between 40.4 and 40.5º W, ranged from ~40 – 110 m deep. The approximately current width was 100 km, and the volume transport was 1.7 Sv (35-120m). However, the flow was not fully measured. The VMADCP reached the maximum depth of 120 m, and at this depth the current was still intense.

3.2 The Intermediate Western Boundary Current Flow

The IWBC was sampled in the VTR region between 19 and 22 °S (Table 3.2, Figure 3.4). Geostrophic and LADCP sections resulted from the data collected during the PNBOIA III, PNBOIA I, and VTR-FLUXES cruises. The PNBOIA III cruise had the current velocities based only on geostrophy, the PNBOIA I cruise had geostrophic and LADCP sections, and the VTR-FLUXES cruise had all sections based on LADCP measurements.

Table 3.2: Volume transport across each of the fourteen sections that captured the IWBC from 19.3 to 21.5°S. Each color represents a different cruise: PNBOIA III (blue), PNBOIA I (red), and Cruzeiro do Sul (green). Figure 3.4 presents the location of each section, and Appendix C shows the vertical sections not presented in sub-section 3.2.

Section Number	Latitude (°S)	Longitude (°W)	Measurement Method	Water Mass Transport (Sv)	Total Transport (Sv)	Month/Year
C1	21.5	39.9 – 39.1	CTD (Geostrophy)	SACW – 3.6 AAIW – 4.1 UCPW – 2.7	11.0	Mar-Apr/2014
C2	21.1	39.8 – 39.4	CTD (Geostrophy)	SACW – 1.0 AAIW - 1.6 UCPW – 0.6	3.3	Feb-Mar/2014
C3	21.1	38.8 – 38	CTD (Geostrophy)	SACW – 1.9 AAIW - 1.4 UCPW – 1.4	4.7	Feb-Mar/2014
C4	20.25	39.8 – 38.6	LADCP	SACW – 3.0 AAIW - 1.6 UCPW – 0.9	5.5	Mar/2014
C5	20	39.6 – 38.8	CTD (Geostrophy)	SACW – 5.2 AAIW - --- UCPW - ---	5.2	Aug/2013
C6	20	37.4 – 36.2	CTD (Geostrophy)	SACW – 8.6 AAIW – 7.7 UCPW – 4.3	20.6	Aug/2013
C7	19.85	38.4 – 36.6	LADCP	SACW – 6.6 AAIW – 2.8 UCPW – 1.0	10.4	Mar/2014
C8	19.45	37.7 – 36.7	CTD (Geostrophy)	SACW – 7.1 AAIW – 7.4 UCPW – 4.8	19.4	Mar/2014
C9	19.3	37.4 – 36.7	CTD (Geostrophy)	SACW – 3.7 AAIW – 3.1 UCPW – 1.8	8.6	Aug/2013
C10	19.6 - 19.3	38.1	LADCP	SACW - 0.3 AAIW - --- UCPW - ---	0.3	Aug/2014
C11	20.5 - 20.1	38.2	LADCP	SACW - 3.8 AAIW - 3.2 UCPW - 0.3	7.3	Aug/2014
C12	20.4 – 20.1	38.7 – 38.35	LADCP	SACW - 2.2 AAIW - 2.1 UCPW - 0.8	4.9	Aug/2014
C13	21.5 - 20.6	38.1	LADCP	SACW - 0.9 AAIW - 1.3 UCPW - 0.3	2.5	Aug/2014

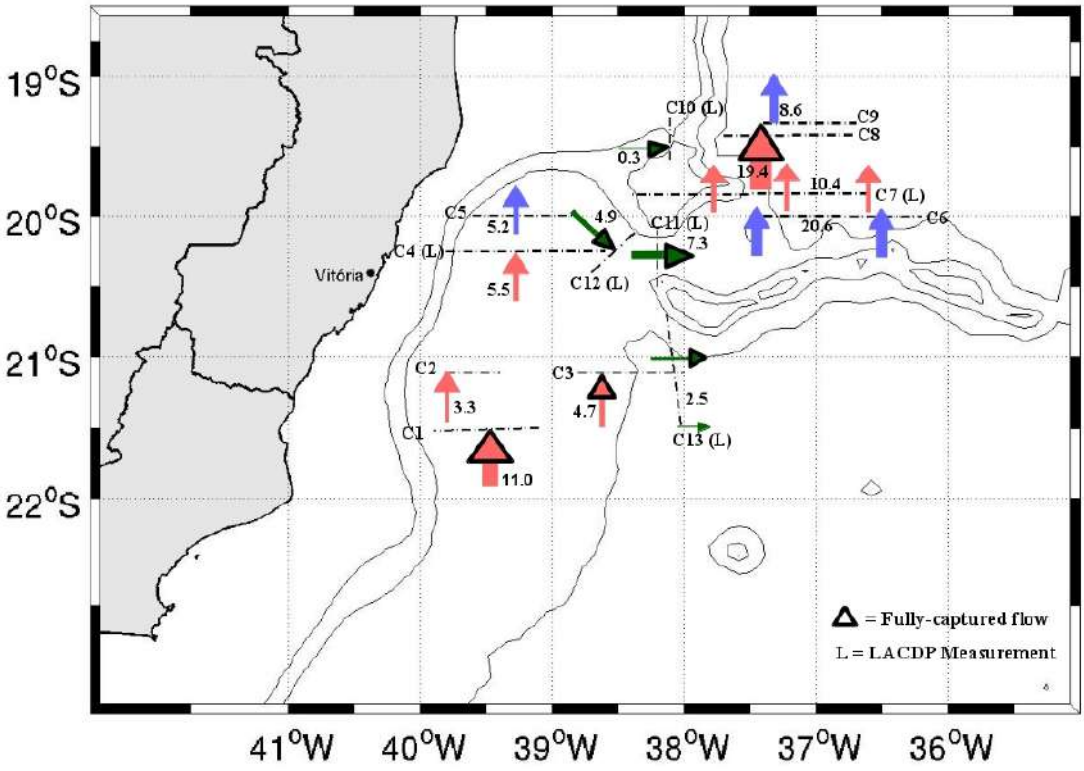

Figure 3.4: Sections (C1 to C14) where the IWBC flows were calculated by geostrophy or LADCP (L) measurements. The arrows thickness are proportional to the IWBC volume, and the arrows positions indicate the IWBC core. Each color represent a different cruise: PNBOIA III (blue), PNBOIA I (red), and VTR-FLUXES (green). The numbers by the arrows represent the total volume transport. The volume transport of each water mass within a section is presented in Table 3.2. The bold triangle indicate that the IWBC flow was fully captured in the section.

The potential density was calculated in order to limit the water masses. Vertical sections revealed the IWBC transporting not only AAIW (σ_θ=27.05 – superior limit), but also SACW (σ_θ=26.00 – superior limit) and UCPW (σ_1=32.00 – superior limit) (Figure 3.2, Table 3.2). The two first water masses had greater importance in the flow composition, and the SACW, when compared to the AAIW and UCPW, had the highest volume transport in most of the sections. The SACW volume was dominant in seven out of eleven sections that presented the three water masses.

The IWBC flow organization pattern varied with the latitude. In the southernmost

region (C1 – Figure 3.4), at 21.5 °S, the IWBC was organized as an unique and intense northward flow at 39.5º W. The maximum current velocity was 31 cm/s, and the presence of a 30 cm/s core was observed between 600 and 800 m deep. Upper north, at 21.1º S, the flow was split into two branches (C2 and C3, Figure 3.4). The east flow was fully captured and transported a total of 4.7 Sv, and the west portion transported the volume of 3.3 Sv. Even thought the number was lower for the last (C2), just approximately half of the flow was measured.

At the Tubarão Bight, the IWBC flow was captured close to the continental slope (C4 and C5 - Figure 3.4) and before it reached the underwater channel between the Vitória Seamount and Besnard Bank (C12 - Figure 3.4). At 20.25 °S (C4 - Figure 3.4), the current volume transport was 5.5 Sv. However, the measurements did not capture the current velocity profile from an important area close to the continental slope, where the IWBC is more intense. There was a blank in the measurements below 600 m, between 39.2 and 39.7°W. For this reason, the contributions of the AAIW and UCPW were underestimated, as well as the total volume (Table 3.2). The maximum meridional velocity was 18 cm/s. Further north, the maximum velocity at 20°S (C5 - Figure 3.4) was 22 cm/s. At this latitude, the IWBC carried 5.2 Sv of SACW. This was the only water mass that was sampled. Near the central channel, a volume transport of 4.9 Sv was observed (C12 - Figure 3.4). The flow headed southeast, the maximum velocity was 33 cm/s, and the 30 cm/s core was located between 20.25 and 20.3°W, ranging from 650 to 750 m deep. In the VTR region, the IWBC used the underwater channels (C10 and C11 - Figure 3.4) and the southernmost path (C13 - Figure 3.4) to deal its way through the barrier imposed by the seamounts.

Between the Abrolhos and the Besnard Banks (C10 – Figure 3.4), the shallowest

depths were observed, and the IWBC carried only SACW (Figure 3.2). Even though the current maximum velocity was intense (49 cm/s), the area between the seamounts was limited, and the volume transport was only 0.3 Sv (Table 3.2). Intense velocities were also found between the Besnard Bank and the Vitória Seamount (C11 – Figure 3.4). The IWBC in this channel reached 44 cm/s. However, differently from the channel between the Abrolhos and the Besnard Banks (C10 – Figure 3.4), in this central channel (C11 – Figure 3.4) the current transported SACW, AAIW, and UCPW. The main water masses transported were SACW and AAIW, and their volume transports were 3.8 and 3.3 Sv, respectively. Within the AAIW range, the 40 cm/s core was found at approximately 700 m. A small parcel of the flow, 0.3 Sv, carried UCPW, and the total volume in the section was 7.3 Sv. This was the highest volume transported by the IWBC through the seamounts paths (C10, C11, and C13 – Figure 3.4). Thus, became evident that the main path used by the current to cross the VTR region was between the Besnard Bank and the Vitória Seamount (C11 – Figure 3.4). The IWBC in this channel ranged from approximately 150 to 1500 m deep.

On the southernmost path through the VTR region (C13 – Figure 3.4), the flow was less intense and spread more broadly. The maximum velocity was 19 cm/s, and the IWBC also transported SACW, AAIW, and UCPW (Figure 3.2, Table 3.2). The two first presented higher volume numbers, but the AAIW was the main water mass transported by the current. The most intense current core of 10 cm/s was located between 700 and 900 m deep, within the AAIW range (Figure 3.2). Differently from what was observed between the Besnard Bank and the Vitória Seamount (C11), the highest velocities were found deeper in the water column, as well as the BC-IWBC direction inversion (Figure 3.2).

From the analysis of the flow through the seamounts region (C10, C11, and C13), the IWBC division into branches to deal with the physical barriers imposed by the seamounts became evident. Such a disorganized pattern was also observed after the flow crossed the VTR region (C6 and C7 - Figure 3.4). In each of these locations, more than one core was observed. At 20 °S (C6 - Figure 3.4), the current cores were located at 36.7 and 37.4°W. While the east core transported 15 Sv, the west core carried 5.6 Sv. However, only approximately half of the west flow was measured. The half sampled ranged from 37 to 37.4ºW, and the flow had maximum velocity of 30 cm/s. The east core was twice as wide, and the maximum velocity was 35 cm/s.

Further north (C7 – Figure 3.4), three cores could be observed. Two of them were positioned in the upper portion water column (at about 250 m), while the third (Figure 3.4 – middle arrow) was between the depths of 600 and 800 m. All of them had maximum core velocities of 20 cm/s, and the total volume transport volume was 10.4 Sv. From 37.2 to 37.8ºW, current measurements of an important area at intermediate depths were not performed. Such measurements would lead to a increase in the volume number, and also to a better understanding of the deeper core flow.

At ~19.5 °S (C8 – Figure 3.4) the flow was fully captured, and the total volume transport was 19.4 Sv. The increase in volume transport when compared to the southernmost IWBC measurement (C1 – Figure 3.4) indicated an intensification of the IWBC on its way north. The maximum velocity at this lower latitude was 38 cm/s, and the 30 cm/s core, centered at 37.35°W, was 0.2° wide, and ranged from 500 to 1300 m deep. The IWBC was intense, and occupied a large area. Also, the current was already organized as an unique flow by the continental slope.

The same pattern was observed at 19.3° S (C9 – Figure 3.4). The organized and

intense pattern of the current was also noticed. The maximum velocity recorded was 35 cm/s, and the 30 cm/s core occupied the depths between 600 and 1150 m. Between 19.3 and 19.5 °S (C8 and C9 – Figure 3.4) the main water masses transported by the IWBC were SACW and AAIW, but the UCPW also had a considerable volume (Table 3.2). The total IWBC volume transport at 19.3 °S was 8.6 Sv (C9 – Figure 3.4), however only approximately half of the current was measured.

3.3 Mesoscale Activity

During the PNBOIA III and the VTR-FLUXES cruises, three eddies were sampled inside the Tubarão Bight. The analysis combined Chla, SST, and MSLA remote sensing data with CTD and VMADCP data measured *in situ*. Remote sensing data were important in the identification of the mesoscale features. Also, this data revealed important information related to the eddies formation, translation, and surface velocities. The *in situ* measured data made possible the description of the eddies' vertical structure. Each eddy is analyzed separately as it follows.

3.3.1 Eddy 1 – July/2013

During the PNBOIA III cruise, a VMADCP section and three oceanographic stations, at approximately 20.6° S, captured a signal associated with a cyclonic eddy near the Vitória Seamount (Figure 3.5). The eddy was sampled *in situ* between July 29 and 30, 2013 (Figure 3.5b and 3.5c). MSLA images revealed that this eddy had been remotely formed near Cape São Tomé (~ 22 ° S). After formation, the eddy migrated northwards and reached the Tubarão Bight (Mill et al., 2015). The vertical section of

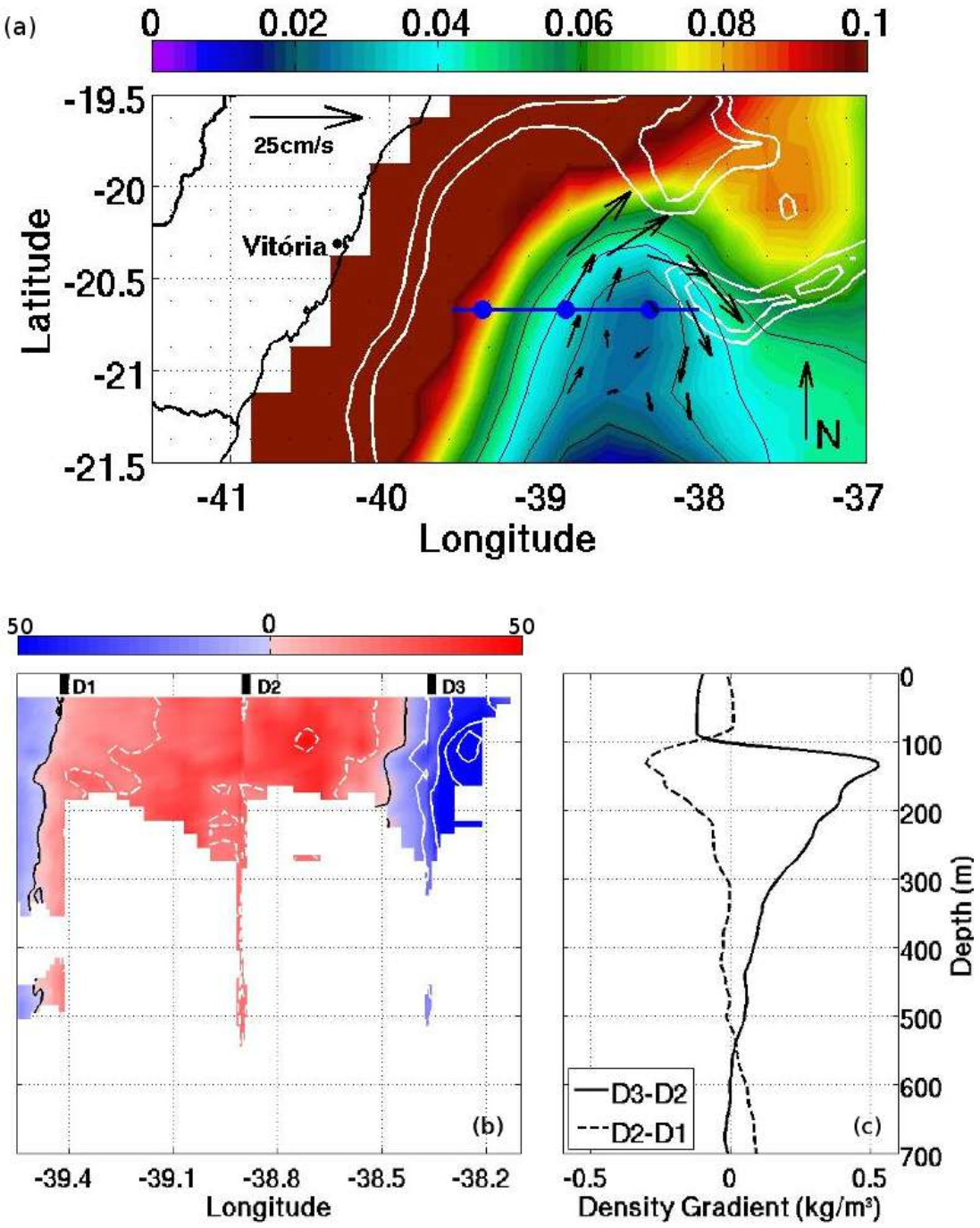

Figure 3.5: (a) Geostrophic velocity anomalies (arrows) on the top of the Mean Sea Level Anomaly (MSLA) image from AVISO 1/4° x 1/4°(m) on July 28, 2013. The blue lines represent the vessel route, and the blue dots represent the hydrographic stations (D1, D2, and D3). (b) Meridional velocities recorded by the VMADCP along the vessel track. (c) Density gradients (kg/m^3) between stations.

meridional velocities captured the final stage of the eddy's life, but its signal was clear from surface down to the maximum depth reached by the VMADCP (~ 300 m - Figure 3.5b). Velocity measurements below 300 m, though isolated, suggested that the eddy was even deeper (Figure 3.5b), which was also described by Mill et al. (2015). This deep-reaching eddy contrasts with the locally formed cyclonic eddy, such as the Vitória Eddy that presents a shallower signal (Schmid et al., 1995). The deeper range of the eddy presented in this work was confirmed by the density profiles measured in July/2013 (Figure 3.5c). The feature deformed the isopycnals down to ~ 550 m deep. The maximum horizontal density variation was 0.5 kg/m^3, near 130 m deep (Figure 3.5c).

A sub-surface velocity core of ~ 80 cm/s was observed near 110 m (Figure 3.5b). This subsurface core was possibly associated with the long eddy life time (~ 3 months). Throughout this time period, before measurements, the mesoscale feature had probably suffered strong atmospheric influence in the first tens of meters. In addition, differently from locally formed cyclonic eddies (item 3.3.3), the surface chlorophyll-a signal was weak. The portion of the eddy that was captured transported 3.6 Sv northwards and 1.5 Sv southwards. The southward portion was only partially measured (Figure 3.5a and 3.5b). This transport volume was higher than the one found for the locally formed cyclone, which was 2.9 Sv (Schmid et al., 1995).

3.3.2 Eddy 2 – August/2013

During the PNBOIA III, in 2013, the signal of a second eddy could be seen in the geostrophic velocity anomalies, VMADCP, and CTD data (Figure 3.6). This anticyclonic eddy, which has already been reported in the region (Arruda et al., 2013),

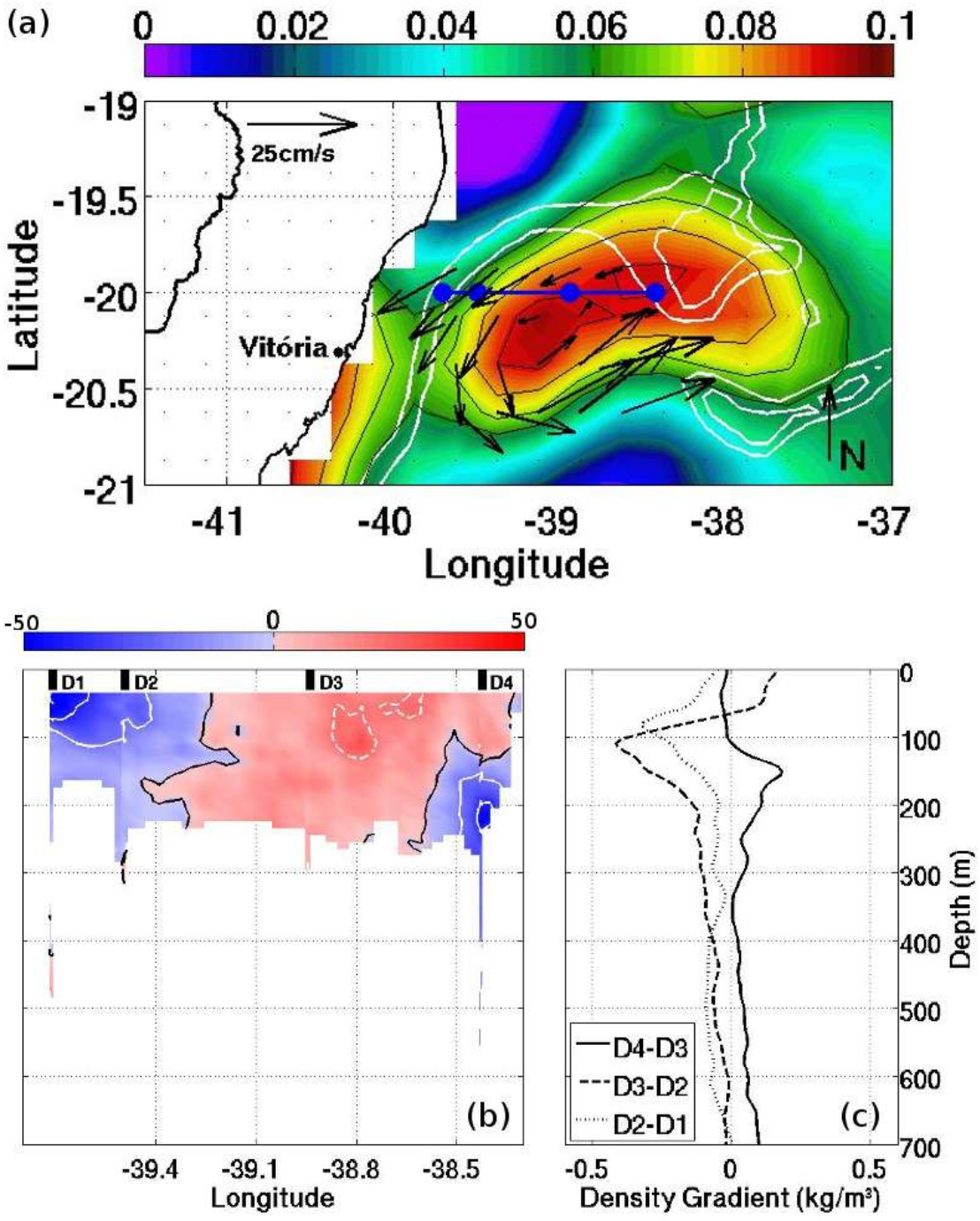

Figura 3.6: (a) Geostrophic velocity anomalies (arrows) on the top of the Mean Sea Level Anomaly (MSLA) image from AVISO 1/4° x 1/4° (m) on August 8, 2013. The blue lines represent the vessel route, and the blue dots represent the hydrographic stations (D1, D2, D3, and D4). (b) Meridional velocities recorded by the VMADCP along the vessel track. (c) Density gradients (kg/m^3) between stations.

was sampled between August 5 and 6. Differently from the section that captured the cyclonic eddy in July, the August section, composed by the oceanographic stations and by the vessel route (VMADCP), did not cross the eddy center (Figure 3.6a). The density variation between stations indicated that the eddy influence on the local density field was restricted to the top 300 m (Figure 3.6c). Within this layer, the northward core was observed around 100 m deep (Figure 3.6b), where the density variation between D3 and D2 reached its maximum (~ -0.45 kg/m^3) . The maximum velocity was 62 cm/s, and the eddy transported 1.5 Sv northwards and 1 Sv southwards in the top 200 m.

3.3.3 Eddy 3 – August/2014

In 2014, a third eddy was sampled during the VTR-FLUXES cruise. The signal of this locally formed eddy was identified due to the combined analysis of VMADCP (Figure 3.7a , and pink arrows on Figure 3.8), SST (Figure 3.8a and 3.8c), and chlorophyll-a (Figure 3.8b and 3.8d) data. Similar to what occurred with the anticyclonic eddy in August/2013, the 2014 section also crossed the periphery of the eddy on August 16 (Figure 3.8). However, the eddy velocity inversion was noticeable (Figure 3.7a), as well as the 20 cm/s core on both sides of the feature. According to the density variation between stations, the mesoscale feature influenced the isopycnals structure down to approximately 200 m (Figure 3.7b), and within this layer the flow transported 1.2 Sv. Not only the depth of influence, as well as the transport volume were smaller than the ones reported by Schmid et al. (1995), which were 350 m and 2.9 Sv.

When compared to the eddy remotely formed near Cape São Tomé, the locally formed eddy was ~350 m shallower. On the other hand, the locally formed eddy presented a more intense chlorophyll-a signal (Figure 3.8b and 3.8d), which evidenced

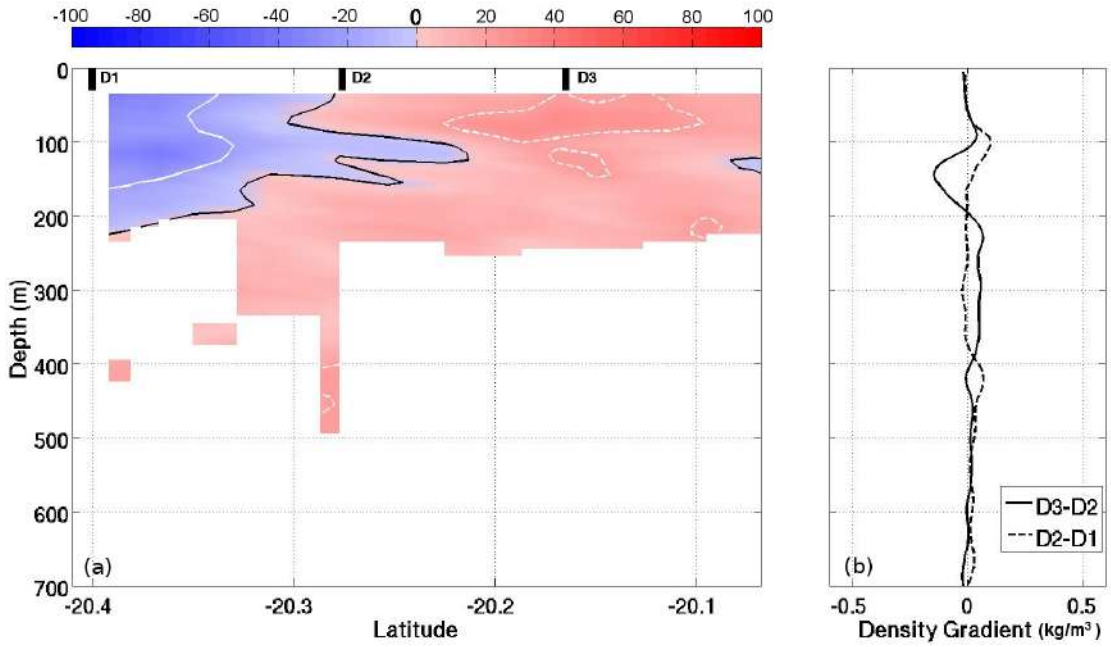

Figura 3.7: (a) Current velocities (cm/s) perpendicular to the section recorded on August 16, 2014, by the VMADCP along the vessel track. (b) Density gradients (kg/m^3) between hydrographic stations.

its biological importance. Figure 3.8 presents an evolution of the feature along the time. The SST images show the BC meandering near the stations (Figure 3.8a) between August 13 and 19, 2014. In the following week, the current advected water around the eddy and threw offshore warmer water near the continental slope at ~20° S, between 39 and 40° W (Figure 3.8c). The consequence of the BC meandering and further eddy formation could be observed on the chlorophyll-a image (Figure 3.8d). High chlorophyll-a concentrations matched up with the eddy geographical location (Figure 3.8d).

Eddies 1 and 2, sampled in 2013, did not present the chlorophyll-a concentration as high as the 2014 eddy (Eddy 3) (Figure 3.9). Chlorophyll-a zonal sections were extracted from MODIS/Aqua sensor data, and the surface concentrations across the

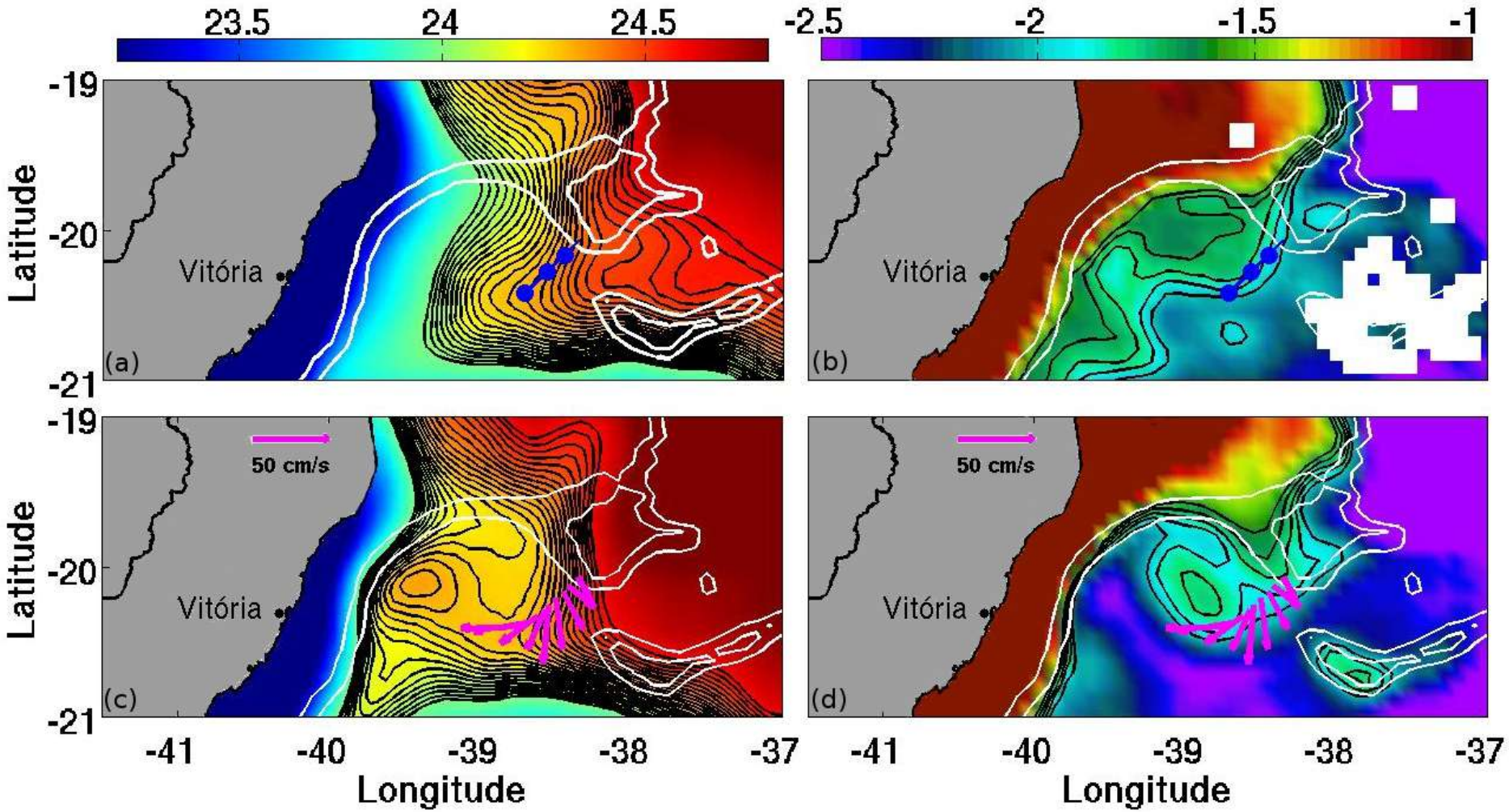

Figura 3.8: Sea Surface Temperature images, as depicted by OSTIA SST (°C), from August 13 to 19, 2014 (a), and from August 20 to 26, 2014 (c). On the right, Chlorophyll-a image from MODIS/Aqua sensor (mg/m^3) from August 13 to 20, 2014 (b), and from August 21 to 28, 2014 (d). The blue line on the top images represent the vessel route, and the blue dots represent the hydrographic stations (D1, D2, and D3 – from left to right). The pink arrows on the bottom images show the average flow (direction and intensity) in the top 100 m of the water column.

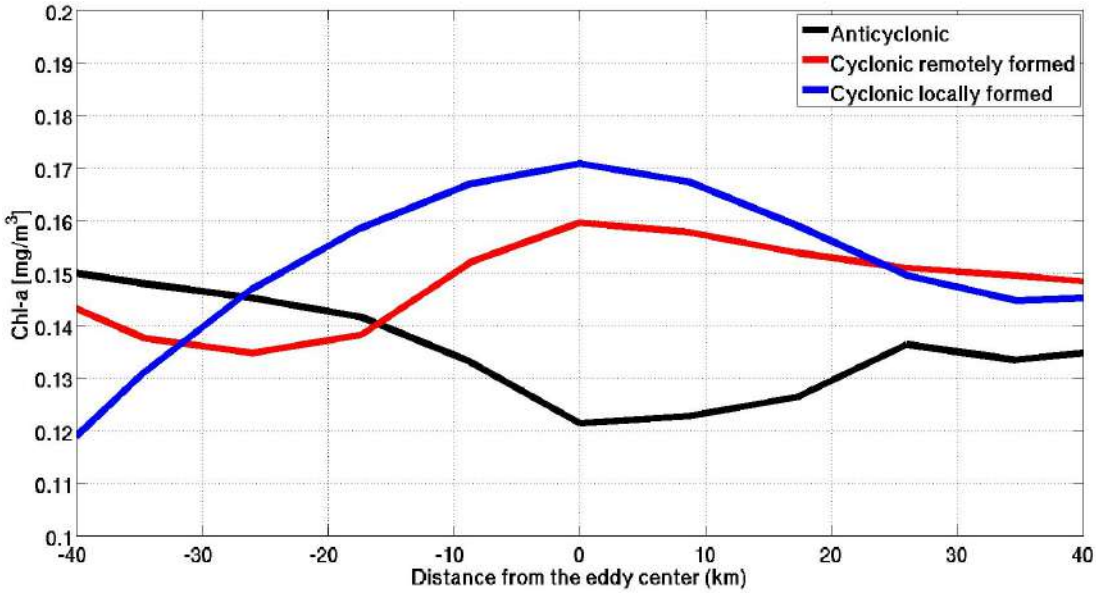

Figura 3.9: Chlorophyll-a concentration (mg/m^3 - MODIS/Aqua sensor) along zonal transects that crossed the eddy center.

eddies could be observed. The two cyclonic features had their highest concentration number at the center of the eddy, and, in both cases, the concentration decreased as the distance from the center increased. The remotely formed cyclonic eddy presented a surface signature less intense (0.16 mg/m^3) than the locally formed cyclonic (0.17 mg/m^3). Both cyclonic features had an increase in chlorophyll-a concentration possibly due to the upward pump of deep rich nutrient waters. Also, the 2014 eddy had a strong influence of rich nutrient coastal waters. The lower concentration in the 2013 cyclonic eddy could be related to the long life of the remotely formed eddy. Due to interactions with the atmosphere and local hydrodynamics, the surface signal could have been attenuated.

The anticyclonic eddy had its lowest chlorophyll-a concentration (0.12 mg/m^3) at the eddy center. In this case, the cyclonic eddy pumped nutrient rich waters to deeper regions in the water column, and as a consequence, a deficit in phytoplankton biomass

was observed. Siegel et al (2011) described this pumping mechanism hypothesis. As the distance from the eddy center increased, the chlorophyll-a concentration also increased.

Chapter 4
Discussion and Conclusion

This study presents an investigation of the BC and IWBC flows through the VTR region. The description of the currents, based on *in situ* measurements between 19ºS and 23ºS, aims to identify the paths of the flows, their volume transport, the water masses carried by the flows, and how they work their way to get through the topographic barrier imposed by the seamounts. The vertical structure of the currents, as well as latitudinal changes in these structures, are discussed.

No clear division of the BC among VTR channels was observed. The current not only crossed the VTR region through the underwater channels, but also over the Besnard Bank and Vitória Seamount (Figure 3.1). The BC flow could be observed as far south as 21.5 ºS, which was the southern most point, near the ridge, crossed by a vessel. The presence of this westward flow to the south of the Vitória Seamount (S16 – Figure 3.3) agreed with Evans and Signorini (1985) observation. The authors reported that part of the BC southward flow was noticed to the east of the Vitória Seamount. This easternmost BC portion, after crossing the complex VTR bathymetry, headed towards the continental slope (S16 – Figure 3.3), possibly in an attempt to adjust its potential vorticity.

As observed by Muller et al. (1998), the BC was also identified as a shallow current near the ridge. The meridional section (Figure 3.2) shows that in August/2014 the BC was not deeper than 300 m. Even though negative zonal velocities were observed down to ~500 m to the south of the Vitória Seamount, the velocities were very

low below 200 m deep. At ~20 °S, the present study found a volume of ~1.0 Sv being transported by the BC (S5 and S6 – Figure 3.3). This volume transport was lower than the volumes found by Evans et al. (1983) (3.8 and 6.8 Sv) for a section at the approximately same latitude. However, Evans et al. (1983) considered 500 and 1000 m, respectively, as levels of no motion. According to the zonal velocities along the water column (Figure 3.2), at these depths, an intense IWBC flow in the opposite direction could be observed. Assuming that this pattern is stable along the time, the BC volume calculated by Evans et al. (1983) was overestimated.

A volume transport closer to the one found in this study, at the approximately same latitude of 20 °S, was found by Stramma et al. (1990). While this work found an average volume transport of 1.0 Sv (S3, S5, and S6 - Figure 3.3), Stramma et al. (1990), registered a southward current of ~2.0 Sv. However, while Stramma et al. (1990) considered that the BC was transporting TW and SACW, the VMADCP measurements in this study were not deeper than 200 m, and the BC transported only TW. In adition, the measurements at 19.85 and 20.25 °S (S3 and S6 – Figure 3.3) exhibited considerable blank gaps in the vertical section. Thus, the transport numbers found in this paper are comparable to the numbers found by Stramma et al. (1990) in the VTR region.

The literature also describes that when the BC flow reaches the VTR region, the current is divided into branches, and becomes disorganized (Evans et al., 1983; Evans and Signorini, 1985). This pattern could also be observed in the measurements near the seamounts (S3, S5, S6, S14, S15, and S16 – Figure 3.3), where the flow was influenced by abrupt changes in bathymetry. In the VTR region, the BC was organized as an unique branch only at 20 °S, to the east of the Besnard Bank (S5 – Figure 3.3). At this location, a subsurface core could be observed at approximately 170 m deep. Subsurface cores

were a recurrent feature in the BC, and could be noticed not only near the seamounts, but also further south (S12 - Figure 3.3). With regard to the BC velocities near the VTR, the measurements agreed well with Evans et al. (1983) results. The maximum velocity recorded at 19.85 °S (S3 – Figure 3.3) was 56 cm/s, and Evans et al. (1983) found 52 cm/s. Further south, the maximum velocity did not reach 40 cm/s (S5 and S6 – Figure 3.3), and through the channels (S14, S15, and S16 – Figure 3.3) a 20 cm/s core was the most intense flow observed. The numbers suggest that as the BC crossed the VTR, the flow not only got divided into branches, but also lost intensity.

A single organized flow was also observed on BC measurements to the north of the VTR (S1 and S2 – Figure 3.3). The volume transports were 0.8 (S1) and 1.0 (S2) Sv, which points to a more intense current in 2014 (S2 – Figure 3.3). In this year, the current flow in the top 100 m transported a higher volume than in 2013 (S1 – Figure 3.3), when the VMADCP measurements reached 200 m. Geostrophic sections (C8 and C9 - Figure 3.4) also indicated a deeper more intense BC in 2014 than in 2013. In 2014, a 40 cm/s core extended from the surface down to 100 m deep (VMADCP range for the section). The maximum velocities were 35 cm/s (S1 – Figure 3.3) and 49 cm/s (S2 – Figure 3.3). Evans et al. (1983), at 19 °S, found a maximum velocity of 50 cm/s and a volume transport of 5.3 Sv, and Miranda and Castro (1981) found 72 cm/s and 6.5 Sv. Even though both volumes were higher than the volumes described in the present study, the two works considered the top 500 m (level of no motion) in their volume transport calculations. However, from the VMADCP and geostrophic sections in this study, we could notice that the BC at ~19 ºS was not deeper than ~200-250 m. Arruda et al. (2013) reached to the same conclusion with their modeling analysis. Also, the authors found the same 40 cm/s BC core at this latitude.

At higher latitudes (below 20 °S), inside the Tubarão Bight, the BC portion that was not flowing by the continental slope (S3, S5, S6, S14, S15, and S16 – Figure 3.3) headed towards the shelf break, and met the coastal BC portion (S4 – Figure 3.3). This BC portion that ran along the continental slope (S4 – Figure 3.3) occupied the top 150 m of the water column, transported 1.0 Sv, and had core velocities that exceeded 50 cm/s. Stramma et al. (1990), at the same latitude and also in the coastal region, found 1.6 Sv of volume and a maximum velocity of 24 cm/s. Further south (S7 – Figure 3.3), a deeper BC could be observed. Such a current deepening is possibly related to the SEC bifurcation in lower levels, which was reported by Stramma and England (1999).

The BC portion that crossed the VTR through the seamounts region (S3, S5, S6, S14, S15, and S16 – Figure 3.3) joined the BC flow that ran along the continental slope (S4 and S7 – Figure 3.3), and got organized as a single flow between 21 and 22 °S. Between these latitudes, the BC flows presented multiple cores (S8, S9, S10, S11, and S12 – Figure 3.3), but further south, at 23 °S (S13 – Figure 3.3), during the PNBOIA I cruise, the current was clearly more intense and organized by the continental shelf break region. At this latitude, the 60 cm/s core was deeper than 100 m, and the volume transport was 1.7 Sv. Even though the volume transport at 22 °S (S12 – Figure 3.3) was higher (3.7 Sv / 35-300 m), at 23 °S (S13 – Figure 3.3) only the top 120 m of the water column could be measured by the VMADCP. Also, at this location, a large blank area was observed in the current measurements. Thus, considering that the BC at this latitude was deeper than 300 m, such as was observed at 22 °S (S12 – Figure 3.3), about a third of the current volume was measured. In this same region, Evans et al. (1983) found 4.4 Sv being transported by the BC at 21.7 °S, Rodrigues et al. (2007) and Signorini (1978) found 6.0 and 5.2 Sv, respectively, at 22 °S, da Silveira et al. (2004) found 5.6 ± 1.2 Sv

at 23 °S, and Campos et al. (1995) found 7.3 Sv just south of 23 °S. The maximum velocities were also comparable to other studies, which ranged from 19 cm/s (Signorini, 1978) to 61 cm/s (Evans et al., 1983).

With regards to the IWBC, the volume proportions of the general circulation agreed with Costa et al. (2017) description, who based their results on lagrangian floats and numerical modeling analysis. According to the authors, from the total IWBC volume that heads north at 23 °S, 70% crosses the VTR region through the channel between the Besnard bank and the Vitória Seamount (C11 – Figure 3.4), and the remaining 30% used the eastward path along the southern flank of the Vitória Seamount (C13 – Figure 3.4). Considering that the present study calculated the volume of 10.4 Sv entering the Tubarão Bight (C1 – Figure 3.4), the volumes of 7.3 Sv (C11 – Figure 3.4) and 2.5 Sv (C13 – Figure 3.4) were comparable to Costa et al. (2017) proportions. The percentage of the eastward flow to the south of the Vitória Seamount (C13 – Figure 3.4) was lower than 30%. However, the southernmost flow portion was not fully captured (Figure 3.2), and an IWBC flow at 21.5 ºS, centered at ~700 m, was only partially measured.

Part of the IWBC flow was captured crossing the seamounts region through the northernmost channel, between the Abrolhos and Besnard Banks (C10 – Figure 3.4). Legeais et al. (2013) suggested that this channel could be a possible IWBC pathway, however this information was not discussed into details. Muller et al. (1998) identified 0.7 Sv of AAIW being transported by the IWBC in the channel, with maximum velocity of 20 cm/s. According to the results of this study, only 0.3 Sv of SACW was transported by the IWBC in the channel, and the maximum velocity was 47 cm/s. The channel depth, according to the current available bathymetry, does not reach 400 m. Thus, the

AAIW would not be able to use this path on its way north since the water mass ranges from ~600 to 1100 m deep in the region. Muller et al. (1998) mooring location in the channel was not at the shallowest region.

The AAIW, as well as the SACW and UCPW could be observed in the preferred IWBC pathway. The channel between the Besnard bank and the Vitória Seamount (C11 – Figure 3.4) is ~2000 m deep and presented the highest IWBC volume transport, as was also observed by Legeais et al. (2013) and Costa et al. (2017). Both studies described that after turning clockwise around the Tubarão Bight, most of the IWBC volume gets into the central channel. Analyzing results from a model, Costa et al. (2017) identified a 40 cm/s core in this channel. A core with the same intensity was noticed in this work (C11 – Figure 3.4). However, before entering the channel (C12 – Figure 3.4), the current velocities did not reach 40 cm/s, indicating that the IWBC was intensified as it got into the channel between the Besnard Bank and Vitória Seamount. In addition, the volume transport was also 2.4 Sv higher between these two seamounts (C11 – Figure 3.4). This fact suggests that the flow in the central channel (C11 – Figure 3.4) was not composed only of water that had turned clockwise around the bight. Part of the water could have come from a branch that bifurcated from the main flow that ran along the continental slope, such as the flow observed far away from the continental shelf at ~21°S (C3 - Figure 3.4).

After crossing the VTR region, the IWBC was noticed as a disorganized current with multiple cores just south of 19.5 °S (C6 and C7 – Figure 3.4). According to Legeais et al. (2013), between 20 and 15 °S, the IWBC becomes weaker and there is no real proof of its presence. On the other hand, Arruda et al. (2013) and Costa et al. (2017) described an organized IWBC by the continental slope at 19 °S, and the present study

found a similar pattern. At 19.45 °S, just north of the Besnard Bank, the IWBC was already organized and very intense (C8 – Figure 3.4). At ~19.4 °S (C8 – Figure 3.4), the IWBC was transporting ~19 Sv of SACW, AAIW, and UCPW. At 19.3 °S (C9 – Figure 3.4), the volume transport was lower, but the measurements captured approximately half of the current. Soutelino et al. (2013) calculated in their numerical simulation a northward transport of 9 Sv at ~19.5 °S. However the authors considered that the IWBC ranged from 400 – 860 m deep. Such a depth range considered part of the SACW and most of the AAIW. Measurements in the present study indicated that the BC was very shallow in the regions. Also, the SACW and the UCPW had important participation in the flow. Thus, if Soutelino et al. (2013) considered a deeper depth range, their volume transport could be comparable to the volume transport of this work. In addition, the current velocities found by Soutelino et al. (2013) were lower than the velocities found in this work. While Soutelino et al. (2013) described a core velocity of 20 cm/s, just like Costa et al. (2017), this work found 30 cm/s, the same IWBC average velocity reported by Boebel et al. (1999).

With regards to the IWBC volume transport, Boebel et al. (1999) calculated an average volume transport of 4 ± 2 Sv, which agreed very well with the volume calculated in the southernmost geostrophic section (C1 – Figure 3.4) of this study, taking into account that Boebel et al. (1999) considered AAIW only. The AAIW volume at 21.5 °S (C1 – Figure 3.4) was 4.1 Sv, and the total volume was 11 Sv. Several studies associate the IWBC only with the AAIW (Boebel et al., 1999; Silveira et al. 2004; Soutelino et al., 2013). However geostrophic, LADCP, and VMADCP sections in the present study indicated an equivalent importance of the SACW in the IWBC flow, and also a large volume of UCPW being transported by the current. Costa et al. (2017)

considered the full current flow in their model, and calculated an IWBC transport of 12 ± 5 Sv at 22.7 °S.

Similarly to the northernmost section (C9 – Figure 3.4), the southernmost measurements (C1 – Figure 3.4) recorded a core velocity of 30 cm/s. Silveira et al. (2004), Rocha et al. (2014), and Costa et al. (2017) observed a mean velocity of ~20 cm/s in the same region. At 21.5 °S (C1 – Figure 3.4), the 30 cm/s core area was smaller than at ~19.4 (C8 and C9 – Figure 3.4). This indicates that the flow was more intense at lower latitudes, evidencing the IWBC intensification on its way north. This intensification could be related to the SEC bifurcation in lower levels at ~20°S (Stramma and England, 1999). The SEC branch that bifurcates northwards possibly joins the IWBC, and the current flow is intensified.

A recurrent mesoscale activity was noticed in the study area, between the latitudes of 19 °S and 23 °S. According to the analysis of the sampled eddies, these mesoscale features influenced the phytoplankton biomass, the density field in the water column, and the ocean circulation in the region. Even though this study identified deformed isopycnals down to ~550 m deep, Mill et al. (2015) observed, in this same area, the eddy influence on the density field and on the ocean velocities down to the depth of 800 m. Thus, the BC and IWBC are subject to the influence of the eddies, when these features are present. Also, the data analysis from different cruises pointed to seasonal changes in the flows. For these reasons, these two ocean currents do not present an unique circulation pattern in the VTR region.

References

ARRUDA, W.Z., CAMPOS, E.J.D., ZHARKOV, V., et al., 2013, "Events of equatorward translation of the Vitoria Eddy", *Cont. Shelf Res.* 70, pp. 61–73.

BOEBEL, O., C., S., ZENK, W., 1997, "Flow and recirculation of Antartic Intermediate Water across the Rio Grande Rise", *Journal of Geophysical Research*, v. 102, pp. 20967–20986.

BOEBEL, O., DAVIS, R. E., OLLITRAULT, M., et al., 1999, "The Intermediate Depth Circulation of the Western South Atlantic", *Geophysical Research Letters*, v. 26, n. 21, pp. 3329–3332.

BROECKER, W.S., 1991. "The Great Ocean conveyor". *Oceanography*. 4, pp. 79–89.

CALADO, L., 2006, "Dinâmica da interação da atividade de meso-escala da Corrente do Brasil com o fenômeno da ressurgência costeira ao largo de Cabo Frio e Cabo de São Tomé, RJ", Tese (Doutorado em Ciências, área de Oceanografia Física) – Instituto Oceanográfico da Universidade de São Paulo. São Paulo. 159 f.

CAMPOS, E., GONÇALVES, J., IKEDA, Y., 1995, "Water mass structure and geostrophic circulation in the South Brazil Bight - summer of 1991", *Journal Geophysical Research Oceans*, v. 100, pp. 18.537–18.550.

COSTA, V.S., MILL, G.N., GABIOUX, M., et al., 2017, "The recirculation of the intermediate western boundary current at the Tubarão Bight – Brazil", *Deep Sea Research I*, v. 120, pp. 48-60.

DENGLER, M., SCHOTT, F.A., EDEN, C., et al., 2004, "Break-up of the Atlantic deep western boundary current into eddies at 8° S" , *Letters to Nature*, v. 432, pp. 1018-1020.

DONLON, C. J., MARTIN,M,. STARK, J.D., et al., 2012, “The Operational Sea Surface Temperature and Sea Ice analysis (OSTIA)”. *Remote Sensing of the Environment.* v.116, pp. 140-158.

EMILSON, I., 1961, “The shelf and coastal waters off Southern Brazil”, *Bolm Instituto oceanográfico*, v. 17(2), pp. 101–112. São Paulo.

EVANS, D., SIGNORINI, S. R., 1985, “Vertical structure of the Brazil Current”, *Nature*, v. 315, pp. 48–50.

EVANS, D., SIGNORINI, S. R., MIRANDA, L. B., 1983, “A note on the Transport of the Brazil Current”, *Journal of Physical Oceanography*, v. 13, pp. 1732–1738.

FIRING, E., GORDON, L., 1990, "Deep ocean acoustic Doppler current profiling", *Current Measurement Technology Committee of the Oceanic Engineering Society*, pp. 192 – 201.

FISCHER, J., VISBECK, M., 1993, "Deep Velocity Profiling with Self-contained ADCPs", *J. Atmos. and Oceanic Technol*., v. 10, pp. 764 -773.

FU, L. L., 1981, “The General Circulation and Meridional Heat Transport of the Subtropical South Atlantic Determined by Inverse Methods”, *Journal of Physical Oceanography*, v. 11, pp. 1171–1193.

GARZOLI, S.L., DONG, S., FINE, R., et al., 2015, “The fate of the deep Western boundary Current in the South Atlantic”, *Deep-Sea Res. I*, v. 103, pp. 125–136.

GORDON, A.L., GREENGROVE, C.H.., 1986, “Geostrophic circulation of the Brazil-Falklandconfluence”, *Deep Sea Res.*, v. 33(5), pp. 573-585.

JOSEPH, A. *Measuring Ocean Currents: Tools, Technologies, and Data*. 2014 ed. Print.

KUHLBRODT, T., GRIESEL, A., MONTOYA, M., et al., 2007, “On the driving

processes of the atlantic meridional overturning circulation", *Rev. Geophys.,* v.45, RG2001.

LEGEAIS, J. F., OLLITRAULT, M., ARHAN, M., 2013, "Lagrangian Observation in the Intermediate Western Boundary Current of the South Atlantic", Deep-Sea Research, v.85 Part II, pp. 109–228. Die stratosphare des Atlantischen Ozeans. Wiss Ergebn. Deutsch.

LE TRAON, P.Y., FAUGERE, Y., HERNANDEZ, F., et al., 2003. "Can we merge GEOSAT follow-on with TOPEX/Poseidon and ERS-2 for an improved description of the Ocean circulation?", *J. Atmos. Ocean. Technol*. v. 20, pp. 889–895.

MARTIN, M.J., HINES, A., BELL, M.J., 2007, "Data assimilation in the FOAM operational short-range ocean forecasting system: a description of the scheme and its impact". *Q.J.R. Meteorol. Soc.*, v.133, pp. 981-995.

MASCARENHAS, A., MIRANDA, B., ROCK, Y., 1971, "A study of the oceanographic conditions in the region of Cabo Frio", *Fertility in the Sea*, v. 1, pp. 285–308.

MILL, G.N., COSTA, V.S., LIMA, N.D., et al., 2015, "Northward migration of Cape São Tomé rings, Brazil", *Cont. Shelf Res*. v. 106, pp. 27–37.

MIRANDA, L. B., CASTRO, B., 1981, "Geostrophic flow conditions at 19 °S", *Ciência Interamericana*, v. 22(1-2), pp. 44–48.

MULLER, T. J., IKEDA, Y., ZANGENBERG, N., et al., 1998, "Direct measurements of the western boundary currents off Brazil between 20 °S and 28 °S", *Journal of Geophysical Research*, v. 103, pp. 5429–5437.

NUÑEZ-RIBONI, I., BOEBEL, O., OLLITRAULT, M., et al., 2005, "Lagrangian circulation of Antarctic Intermediate Water in the subtropical South Atlantic", *Deep-Sea Res. II*, v. 52, pp. 545–564.

PETERSON, R. G., STRAMMA, L., 1991, "Upper-level circulation in the South Atlantic Ocean", *Prog. Oceanogr.*, v. 26, pp. 1–73.

REID, J.L., NOWLIN JR, W.D., PATZERT, W.C., 1977, "On the characteristiVTR-FLUXES and circulation of the southwestern Atlantic Ocean", *Journal of Physical Oceanography*, v. 7(1), pp. 62-91.
REID, J.L., 1989, "On the total geostrophic circulation of the South Atlantic Ocean: flow patterns, tracers, and transports", *Prog. Oceanogr.*, v. 23, pp. 149–244.

ROCHA, C.B., SILVEIRA, I.C.A., CASTRO, B.M., et al., 2014. "Vertical structure, energetics, and dynamics of the Brazil Current System at 22°S–28°S", *J. Geophys. Res.*, v. 119, pp. 52–69.

RODRIGUES, R., ROTHSTEIN, L. M., WIMBUSH, M., 2007, "Seasonal variability of the South Equatorial Current Bifurcation in the Atlantic Ocean: A Numerical Study", *Journal of Physical Oceanography*, v. 37, pp. 16–30.

ROEMMICH, D., 1983, "The Balance of Geostrophic and Ekman Transport in the Tropical Atlantic Ocean", *Journal of Physical Oceanography*, v. 13, pp. 1534–1539.

SCHMID C., 1998, "Die Zirkulation des Antarktischen Zwischenwassers im Südatlantik" , Ph.D. Thesis, University of Kiel, Kiel, Germany.

SCHMID, C., GARZOLI, S., 2009, "New observations of the spreading and variability of the Antarctic Intermediate Water in the Atlantic", *Journal of Marine Research*, v. 67, pp. 815–843.

SCHMID, C., SCHAFER, H., PODESTA, G., et al., 1995, "The Vitória Eddy and its relation to the Brazil Current", *Journal of Physical Oceanography*, v. 25, pp. 2532-2546.

SIEGEL, D.A., PETERSON,P., MCGILLICUDDY, J.R., et al., 2011, "Bio-optical

footprints created by mesoscale eddies in the Sargasso Sea", *Geophys. Res. Let.*, 38:L13608.

SIGNORINI, S. R., 1978, "On the circulation and the volume transport of the Brazil Current between the Cape of São Tom´e and Guanabara Bay", *Deep-Sea Research*, v. 25, pp. 481–490.

SILVEIRA, I. C. A., CALADO, L., CASTRO, B. M., et al., 2004, "On the baroclinic structure of the Brazil Current-Intermediate Western Boundary Current system at 22 ° -23 ° S", *Geophysical Research Letters*, v. 31, pp. L14308.

SILVEIRA, I. C. A., LIMA, J., SCHMIDIT, A., 2008, "Is the meander growth in the Brazil Current system off Southeast Brazil due to baroclinic instability", *DynamiVTR-FLUXES of Atmospheres and Oceans*, v. 45, pp. 187–207.

SOUTELINO, R. G., DA SILVEIRA, I.C.A, G. A., MIRANDA, J., 2011, "Is the Brazil Current eddy-dominated to the north of 20 ° S?", *Geophysical Research Letters*, v. 38, pp. L03607.

SOUTELINO, R.G., GANGOPADHYAY, A., DA SILVEIRA, I. C. A., 2013, "The roles of vertical shear and topography on the eddy formation near the site of origin of the Brazil Current", *Cont. Shelf Res.*, v.70, pp. 46–60.

STARK, J.D., DONLON, C.J., MARTIN, M.J., et al., 2007, "OSTIA : An operational, high resolution, real time, global sea surface temperature analysis system", *Oceans '07 IEEE Aberdeen*, Conference Proceedings. Marine challenges: coastline to deep sea. Aberdeen, Scotland.IEEE.

Stommel, H. M., 1958, "The Gulf Stream: a physical and dynamical description". Univ of California Press. pp. 170.

STRAMMA, L., 1989, "The Brazil Current transport south of 23°S", *Deep-Sea*

Research, v. 36, pp. 639-646.

STRAMMA, L., PETERSON, R.G., 1990, "The South Atlantic Current", *J. Phys. Oceanogr*., v. 20, pp. 846-859..

STRAMMA, L., IKEDA, Y., PETERSON, R.G., 1990, "Geostrophic transport in the Brazil Current region north of 20°S", *Deep-Sea Research*, v. 37, pp. 1875-1886.

STRAMMA, L., ENGLAND, M., 1999, "On the water masses and mean circulation of the South Atlantic Ocean", *Journal of Geophysical Research*, v. 104, n.C9, pp. 20.863–20.883.

STRAMMA, L. A., 1995, "The North Brazil Undercurrent." *Deep-Sea Research I*, v. 42, pp. 773–795. Die stratosphare des Atlantischen Ozeans. Wiss Ergebn. Deutsch.

SUGA, T., TALLEY, D., 1995, "Antartic Intermediate Water circulation in the tropical and subtropical South Atlantic", *Journal of Geophysical Research*, v. 100, pp. 13.441-13.453.

SVERDRUP, H. U., JOHNSON, M. W., FLEMING, R. H., 1942, "The Oceans: their physiVTR-FLUXES, chemistry and general biology", *Englewood Cliffs*, p. 1087. Prentice-Hall Inc.

Talley, L.D., 1996, "Antarctic Intermediate Water in the South Atlantic", *The South Atlantic: Present and Past Circulation*, G. Wefer, W. H. Berger, G. Siedler and D. J. Webb, Eds., Springer-Verlag, pp. 219–238.

TSUCHIYA, M., 1985, "Evidence of a double-cell subtropical gyre in the South Atlantic Ocean." *J.Mar Res*., v. 43(1), pp. 57–65.

Visbeck, M., 2002, "Deep velocity using acoustic doppler current profilers: botton track and inverse solutions", *J Atmos Oc Tech*, v. 19, pp. 794–807.

WARNER, M., WEISS, R., 1992, “Chlorofluoromethanes in the South Atlantic Antarctic Intermediate Water.” *Deep-Sea Research*, v. 39, pp. 2053–2075.

WUST, G., 1935, “Schichtung und zirukation des Atlantischen Ozeans”, *Atlant. Exp. Meteor*, v. 6, pp. 109–228. Die stratosphare des Atlantischen Ozeans. Wiss Ergebn. Deutsch.

Appendix A

Bibliographic Revision

A.1 Ocean circulation overview off the eastern Brazilian coast

The ocean circulation off the eastern Brazilian coast is characterized by a complex depth-dependent current system. In the upper-level, the Brazil Current (BC) composes the western limb of the wind-driven South Atlantic Subtropical Gyre (SASG) (Figure A.1). After the bifurcation of the southernmost branch of the South Equatorial Current (SSEC) between between 10ºS and 14ºS, the BC is formed (Peterson and Stramma, 1991; Stramma and England, 1999; Rodrigues et al., 2007). From that point on, the current flows southward. However, the SEC does not reach the Brazilian coast proximity at the same latitude in all depth levels (Stramma and England, 1999) (Figure A.2). Between the depths of 100 and 500m, depth where the South Atlantic Central Water (SACW) is found, occurs a bifurcation at approximately 20ºS. At this latitude, while part of the flow turns southward and thickens the BC, another portion of the water mass goes northward and forms the North Brazil Under Current (NBUC). Below this layer, in the intermediate level (about 500 to 1200 m), the Intermediate Western Boundary Current (IWBC) is formed at circa 28ºS, at the Santos Bifurcation (Boebel et al, 1997). As the current flows northward, it transports mainly Antarctic Intermediate Water (AAIW). However, from the point where the IWBC is formed, before it reaches the Vitória-Trindade Ridge (VTR) region, the layer thickness undergoes changes, and its upper boundary can reach 200m below the ocean's surface (Costa et al., 2017). Thus, a

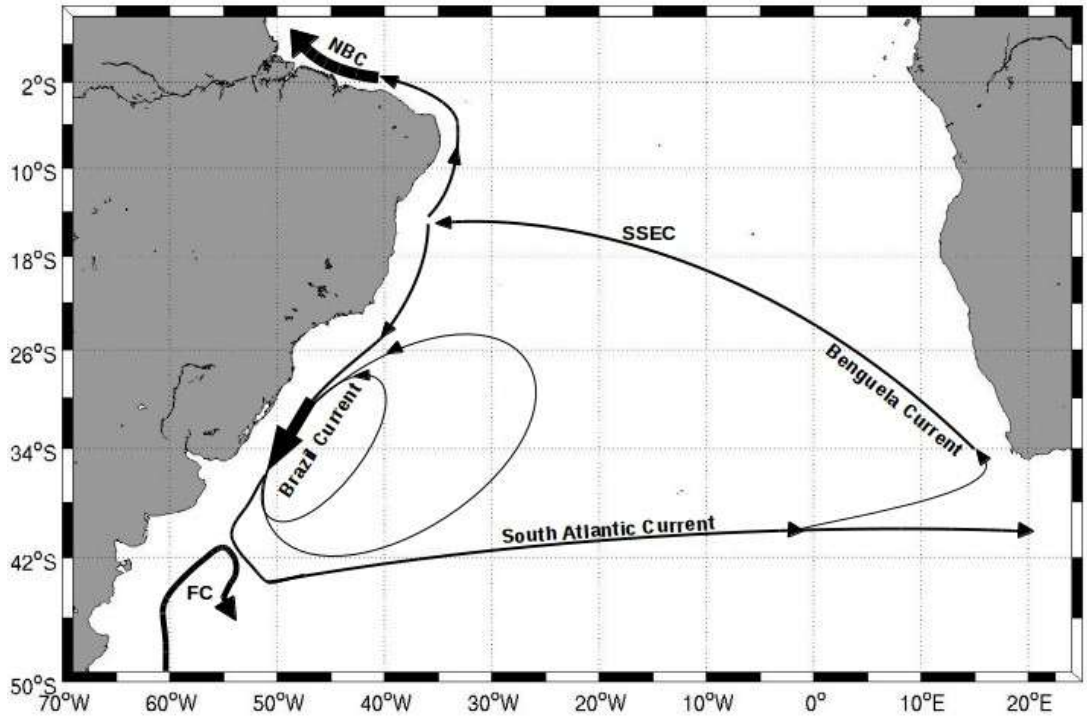

Figure A.1: Wind-driven South Atlantic Subtropical Gyre (SASG). Shown are the North Brazil Current (NBC); the southernmost branch of the South Equatorial Current (SEC); the Brazil Current; the Benguela Current; the South Atlantic Current; and the Falkland Current (FC);

large SACW volume can also be transported by the IWBC. Just as in the case of the surface SEC, after the bifurcation in intermediate level, the southward limb thickens the BC. Only near the depth of 2000m there is an ocean layer that does not change directions along the eastern Brazilian coast. At this depth, the Deep Western Boundary Current (DWBC) carries mainly North Atlantic Deep Water (NADW) along the western South Atlantic (Stramma and England, 1999).

In addition to this complex circulation system, these ocean currents also form and interact with mesoscale features and bottom topography along their way. Currents on the surface (Schmid et al., 1995; Soutelino et al., 2011; Mill et al., 2015), intermediate (Costa et al., 2017; Legeais et al., 2013), and deep (Garzoli et al., 2015; Dengler et al.,

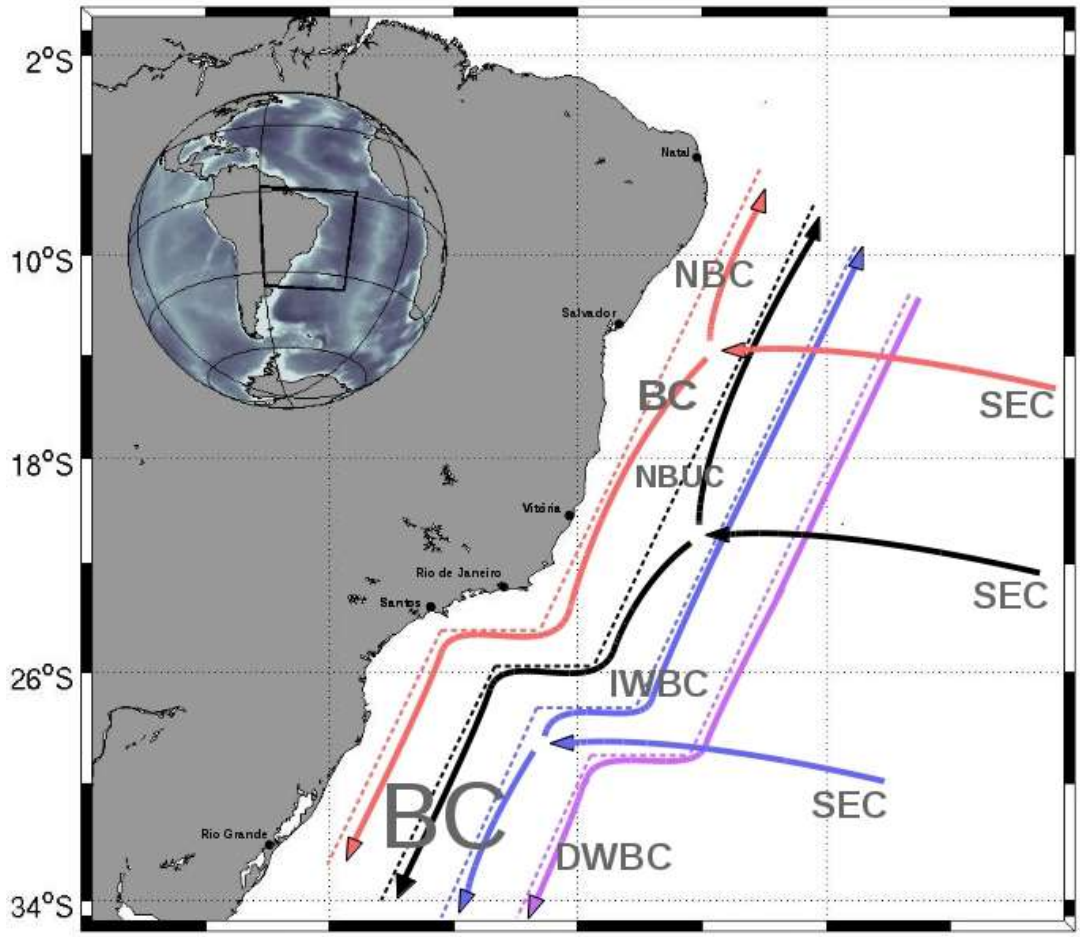

Figure A.2: South Atlantic Western Boundary Currents system. The dashed lines represent the schematic isobathymetric lines of 100 (red), 200 (black), 500 (blue), and 2000 (purple) m. The SEC reaches the South Atlantic western boundary proximity at different latitudes in different depth levels: surface (red), 100-500 m (black), 500-1200 m (blue), and ~2000 m (purple).

2004) levels interact with mesoscale features. Such an interaction causes vigorous changes in the currents flows. The bathymetry also greatly influence these paths (Costa et al., 2017). From the Equator, down to approximately 20ºS, the Royal Charlotte and Abrolhos banks are the most prominent topographic features that guide ocean currents. However at circa 20ºS, a massive zonal physical barrier known as VTR significantly affects the flow from Tropical Surface Water down to NADW (Fu, 1981). Thus, the BC and IWBC flow directions are highly influenced by submerged seamounts in the VTR

region, where the peaks at a few hundred meters in depth contrast with valleys thousands of meters deep.

A.2 The Brazil Current

The BC presents distinct features along its way down the eastern Brazilian coast. After the bifurcation of the southernmost branch of the SEC in the upper 100 m, only 4.1 Sv of the flow turn south to generate the BC (Stramma et al.,1990). Peterson and Stramma (1991) explain that a large portion of water from the northern limb of the South Atlantic subtropical gyre is lost to the northern hemisphere and to equatorial counter currents after the bifurcation. For such a reason, the surface water volume that runs southward along the eastern Brazilian coast is lower than the volumes that are carried by other western boundary currents around the world. In addition, Stommel (1958) attributes that the BC is considerably weak due to the fact that the wind driven component has opposite direction in relation to the thermohaline circulation. Near the generation site, the current is defined as shallow and weak (Stramma and England, 1999; Soutelino,2011). The main water masses transported are Tropical Water and a portion of South Atlantic Central Water (Emilson, 1961; Stramma and England, 1999).

In higher latitudes, between 10 and 20 °S, the BC features present geographic and temporal changes. According to Stramma et al. (1990), there is no intensification pattern from 10 to 20 °S. Analyzing several zonal sections, the authors found the maximum velocities varying between 5 and 60 cm/s, and the transports were between 0.8 and 6 Sv. The maximum transport was at the 19 °S. Other studies calculated volume transport for the BC at the same latitudinal line (Miranda and Castro, 1981; Evans et al., 1983). While Miranda and Castro (1981) found a volume of 6.5 Sv, Evans et al (1983) had a

water volume of 5.3 Sv crossing the section heading southward. Temporal and seasonal transport changes may be attributed either to geographical variability of the SEC bifurcation, which is mainly related to wind variation (Rodrigues et al., 2007), or to interactions between the BC and mesoscale features (Soutelino et al., 2011).

When the BC reaches the VTR region, the flow not only interacts with mesoscale features, but also has to deal its way through the underwater channels created by the seamounts. Soutelino et al. (2011) described the presence of a recurrent anticyclonic eddy just north of the VTR clearly influencing the ocean circulation in the region. Schmid et al. (1995) also reported an eddy formed to the south of the VTR. However, the last was a cyclonic eddy (Vitória Eddy), which was observed crossing the seamounts area during translation. Arruda et al. (2013), in a span of seventeen years, detected six events when the Vitória Eddy translated northwards and crossed the VTR. Despite evidences that the BC flow is highly susceptible to many local factors, oceanographic cruises have also been carried out in a attempt to characterize the ocean current around 20 °S (Evans et al., 1983; Evans and Signorini, 1985). Such studies identified most of the BC flow crossing the seamounts through the channel between the Besnard Bank and Vitória Seamount (Figure 2.1) (Evans et al., 1983) and the presence of the current between the Vitória and Montague seamounts (Evans and Signorini, 1985). Thus, a BC bifurcation was observed in the region.

Even though the split of the flow suggests a local BC disorganization, the current tends to be reorganized close to the continental slope after crossing the VTR (Evans et al., 1983). The mechanism that promotes such organization is the conservation of potential vorticity, which is also responsible for the formation of meanders and eddies reported south of 20°S (Mascarenhas et al., 1971; Signorini, 1978; Calado 2006;

Silveira et al., 2008; Mill et al., 2015). As the current moves towards higher latitudes, the flow becomes deeper and more intense (Evans et al., 1983; Muller et al., 1998; Rocha et al., 2014) due to the merge of the BC with southward flows (after bifurcation) from the SEC in deeper layers. Muller et al. (1998) showed that at 28°S the current was 670 m deep, with a poleward transport of 16 Sv. Other authors highlight the intensification of the BC before it reaches the ending point at the Brazil-Malvinas Confluence region. A recirculation cell at about 30°S is responsible for such intensification (Reid et al., 1977; Tsuchiya, 1985; Gordon and Greengrove, 1986; Stramma, 1989).

A.3 The Intermediate Western Boundary Current

Such as the BC, the IWBC also presents a complex circulation scheme in the South Atlantic. However, differently from the BC, the IWBC transports a portion SACW and mainly AAIW. This water mass is characterized by a low salinity signature, which ranges from 34.2 to 34.6, temperatures between 3 and 6 °C (Sverdrup et al., 1942), and high oxygen levels (Wüst, 1935). Although the AAIW in the South Atlantic originates mainly from surface waters in the Drake Passage and Malvinas Current loop (Talley, 1996), its tongue-shaped salinity minimum (S~34.4) signature can be detected in most meridional hydrographical sections to the north of the Subantarctic Front (Costa et al., 2017).

In order to understand the AAIW spreading by the IWBC in the South Atlantic, researchers have been studying the current for decades. According to the first study related to the current, the AAIW was supposed to go equatorward as a continuous meridional flow along the Brazilian coast (Wüst, 1935). However, years later, studies

based on hydrographic and tracer data proved the AAIW transport in the South Atlantic to be much more complex (Reid, 1989; Warner and Weiss, 1992; Suga and Talley, 1995; Nuñez- Riboni et al., 2005; Schmid and Garzoli, 2009). These authors affirmed that the water in intermediate level undergoes the wind driven circulation of the subtropical gyre, south of ~20ºS. Only when the water mass returns to the southwestern South Atlantic, at ~28ºS, that the IWBC begins (Boebel et al, 1997).

As the westward limb of the subtropical gyre reaches the proximity of the Brazilian continental slope and bifurcates, most of water volume turns to south to close the gyre, and a narrow IWBC heads northward. According to Schmid and Garzoli (2009), about only one-third of the transport volume goes equatorward. From 28ºS to 2ºS, Boebel et al. (1999) described the IWBC as a quasi-continuous flow with the mean speed of 30 cm/s. The study found a northward transport of 4±2 Sv, considering 30±5 km of current width (Schmid, 1998) and 400 m of current depthness (Boebel et al, 1997). Even though such transport estimation fell in the lower limit of the transport range found by Fu (1981), Roemmich (1983), and Silveira et al. (2004) at 22-24ºS (4-8 Sv), the authors added up that the number compared well with the transport calculated by Schmid (1998). Also at 24ºS, Schmid(1998) found a volume of 2.7 Sv, which increased further north. The transport was 4 Sv at 21ºS and 7.7 Sv at 19ºS. Likewise, Legeais et al. (2013) noticed a flow intensification from 27°S to the VTR at 20.5ºS.

Also, before reaching the VTR, the IWBC recirculates, and interacts with mesoscale features (Boebel et al., 1999; Mill et al., 2015; Costa et al., 2017). While Mill et al (2015) described a surface eddy influencing the ocean circulation down to 800 m deep, Costa et al. (2017) reported the presence of a semi-permanent recirculation cell uncoupled from the surface within the Tubarão Bight, to the west of the VTR.

According to Costa et al. (2017), 1/3 of the IWBC flow recirculated within the bight. From the 2/3 left, 70% of the flow crossed the VTR region through the central channel, between the Besnard Bank and the Vitória Seamount, and 30% passed eastward just south of the Vitória Seamount (Figure 2.1). Thus, according to this study, the channel between the Besnard Bank and the Vitória Seamount was the main IWBC route through the seamounts. Such results agreed with Legeais et al. (2013) conclusions, but did not agree with Muller et al. (1998) observations. While the latter reported higher IWBC velocities in the western most channel, between the Abrolhos and Besnard banks, the former computed most of the lagrangian floats, carried by the current at 800m, crossing the region through the central channel. A total of 7 out of 11 floats, after circling clockwise the continental slope around the Tubarão Bight, chose the same main pathway addressed by Costa et al. (2017). Another 2 floats followed the southernmost route to the south of Vitória Seamount.

Due to the irregular bathymetry at the VTR, the IWBC becomes very weak after the crossing the region. From 18ºS to 15ºS the intermediate current is disorganized and dominated by intense mesoscale variability (Legeais et al., 2013). North of this latitude range, the IWBC is reorganized and increases flow along the smooth bottom topography before reaching around 10ºS, where the current faces again a complex bathymetry, and meets the equatorial current system. From that point on, the intermediate water is thought to warm and upwell to feed North Atlantic deep convection and Nordic Seas inflow (Boebel et al.,1999). However, the water mass paths are not yet well understood.

Appendix B

Data Processing

B.1 Themohaline (CTD)

Several processing steps must be taken before the achievement of a CTD final product. The processing steps aim to obtain a consistent, spike free data set. The SBE Data Processing (Seabird) software was used as an initial tool. At first, the software provided support for the data conversion. The raw data recorded by the equipment as an electric tension was converted into oceanographic variables. After the conversion, spikes were commonly observed. Such errors are present in the data due to water turbulence, water flow variations through the sensors, electronic fails, and due to the fact that sensors present different answer times. In order to eliminate spurious and grossly incorrect data, a low-pass filter was applied to the CTD data of each hydrographic station. Thus, derived variables, such as salinity, were obtained.

The following step consisted of the averaging of variables within the bins. Averages were made for every pressure variation of 1 dbar. By then, the parameters profiles presented a considerably organized distribution along the water column. However, before reaching the final product used during the analysis, another low-pass filter was used. The data were filtered by the moving average method, and the moving average span was 5. Figure B.1 exemplifies real temperature curves of a hydrographic station. While the blue line represents the CTD product before the moving average filtering, the red line represents the final product used for the study analysis.

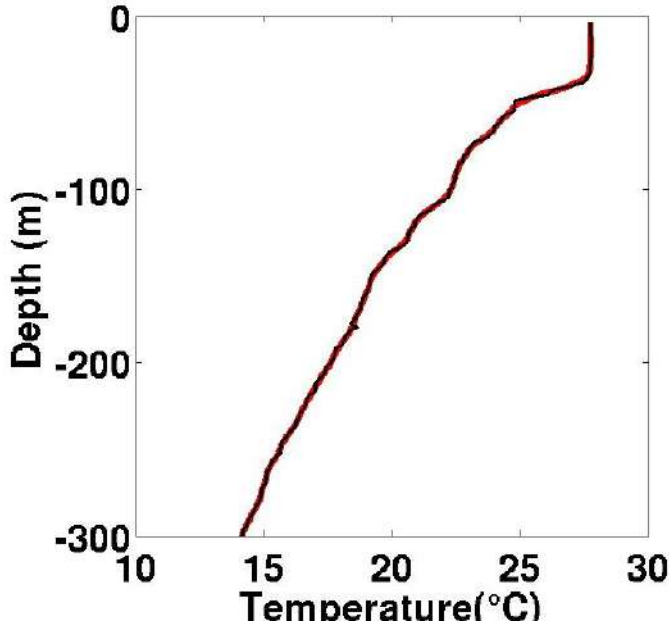

Figure B.1: Temperature profiles of the top 300 m of a hydrographic station. Lines represent the temperatures before (black) and after (red) the moving average filter application.

B.2 Vessel- Mounted Acoustic Doppler Current Profiler (VMADCP)

The VMADCP, such as any current meter based on the Acoustic Doppler principle, measures currents by the transmission of frequency pulses. The transducers send acoustic pulses, and the equipment determines the Doppler frequency shift of the backscattered signal. By this shift, the current speed and direction are calculated. The signal may be backscattered by any kind of inhomogeneity in the water that flow along with the current at the same speed of water particles. The main inhomogeneities in the ocean water column are suspended particulate matter and minute air bubbles.

VMADCP devices are fixed directly in the vessel's hull, and profile currents in the upper ocean along the vessel's path. In order to calculate the absolute current direction and velocity, the VMADCP data processing must take into account several additional

cruise information. This study made use of the Common Ocean Data Access System (CODAS) software to generate VMADCP products. The CODAS tool was developed by the Currents Group, at the University of Hawaii, leaded by Dr. Eric Firing. The processing tools are composed by a suite of open-source programs that use the ancillary information in conjunction with relative current measurements to achieve an absolute current result. The ancillary data encompasses ship's gyrocompass, GPS, and navigation data. The first provides heading information, which is used in the rotation of relative velocities. Thus, the velocity measured by the instrument is rotated to earth's reference frame. After this step, the final velocity components ($\mathbf{u_f}$, $\mathbf{v_f}$) are a combination of the ship's velocities ($\mathbf{u_s}$, $\mathbf{v_s}$) and the velocities measured by the VMADCP ($\mathbf{u_{VMADCP}}$, $\mathbf{v_{VMADCP}}$) (Equations B.1 and B.2).

$$u_f = u_s + u_{VMADCP} \quad \text{(B.1)}$$

$$v_f = v_s + v_{VMADCP} \quad \text{(B.2)}$$

The data submitted to the CODAS processing followed basic steps. First, the software scanned the raw data to ensure they were readable, to check for problems, and to extract recorded profile times. After that, the data was loaded into the analysis database, statistically diagnosed, and plotted. Parameters such as signal strength, *percent good* pings, error velocity were calculated. Signal strength refer to the echo returning intensity from the scatterers, and *percent good* ping is a quality parameter that correlates information from the four transducers. This study considered only VMADCP data above 30 as *percent good*. The following steps edited the profiles and the navigation when necessary, and calibrated the profiler-gyrocompass combining it with the ship's heading. The calibrations had to be determined as a function of time to be

used to correct the velocity data. In addition, another important factor needed to correct the current velocity was ship's velocity. Thus, the ship's average velocities during the profiles were calculated by the ship's position at beginning and at the end of each profile divided by the time difference. Lastly, the depth was adjusted, taking into account the local water density, and the data was gridded for visualizations.

The VMADCP data analyzed in the present work were recorded by a 75 kHz RD Instrument, and the equipment configuration was the same for the three cruises. Due to the equipment frequency, the signal could reach the depth of 400m. However, on average, the upper 200m was more regularly sampled. The bins were 8m long, the ping interval was 3 seconds, and Long Term Averages (LTA) data were used during processing steps. After processing, the final product was gridded in 10m depth intervals and time spans of 15 minutes.

B.3 Lowered Acoustic Doppler Current Profiler (LADCP)

The LADCP data processing followed the procedures described by Visbeck (2002). Thus, absolute current velocities were calculated by the *velocity inversion method.* According to the method, the basic LADCP equation:

$$\boldsymbol{U}_{adcp} = \boldsymbol{U}_{ocean} + \boldsymbol{U}_{ctd} + \boldsymbol{U}_{noise} \tag{B.3}$$

can be thought of as a set of linear equations:

$$\boldsymbol{d} = \boldsymbol{G}\boldsymbol{m} + \boldsymbol{n} \tag{B.4}$$

Where $\mathbf{U_{adcp}}$ represents each ADCP velocity observation, $\mathbf{U_{ocean}}$ is the absolute ocean current velocity, and $\mathbf{U_{ctd}}$ is the motion of the ADCP that is fixed to the rosette. In Equation B.4, **d** represents all $\mathbf{U_{adcp}}$ velocities along the water column, **n** is the measurement noise, **G** is the model matrix, and **m** is a vector that combines unknown ocean velocities and the motion of the CTD package along the profile (Equation B.5).

$$\boldsymbol{m} = \begin{bmatrix} m_{ctd} \\ m_{ocean} \end{bmatrix} \tag{B.5}$$

In order to solve the system in Equation B.6, the least squares methods are applied. These approaches seek to minimize the squared differences between the measured data (**d**) and the predicted data ($\mathbf{d_{pre}}$). The predicted data is an estimation of the model parameter **m**

$$\boldsymbol{G m_{est}} = \boldsymbol{d_{pre}} \quad , \tag{B.6}$$

and $\mathbf{m_{est}}$ is calculated in two different ways in this case:

$$\boldsymbol{m_2^{est}} = [\boldsymbol{G^T G}]^{-1} \boldsymbol{G^T d} \tag{B.7}$$

$$\boldsymbol{m_1^{est}} = \boldsymbol{G^T} [\boldsymbol{G\, G^T}]^{-1} \boldsymbol{d} \tag{B.8}$$

While the parameter $\mathbf{m_2^{est}}$ is the familiar least square solution, the $\mathbf{m_1^{est}}$ is an estimation achieved by a robust method, which is used when a large number of outliers are expected. Since the $\mathbf{m_{est}}$ calculations are different, the prediction errors are respectively:

$$\boldsymbol{E_2} = \sum_{i=1}^{N} \left(\boldsymbol{d_i} - \boldsymbol{d_i^{pre}} \right)^2 \tag{B.9}$$

$$E_1 = [\sum_{i=1}^{N} |(d_i - d_i^{pre})|]^2 \quad \text{(B.10)}$$

The application of the velocity inversion method also allows the addition of auxiliary data into the linear equations. Differently from the shear method (Firing and Gordon,1990; Fischer and Visbeck, 1993), which takes into account only the bottom track information (when available) during the processing steps, the velocity inversion method can combine numerous additional data. Due to the least squares methods, these additional data can be used to constrain the solution (Visbeck, 2002). Data of bottom track, CTD, VMADCP, and GPS are combined with LADCP measurements of two heads (up- and down-looker data) during the processing steps. The clocks synchronization of the equipments is required for the achievement of a high quality product.

Each auxiliary data type plays an important part for the obtainment of the final product. One of the main problems with LADCP data that is processed without CTD time-series is the absence of depth measurements. In these cases, the depth is obtained by the integration of the measured vertical velocities. However, when CTD data is taken into account during processing, a simple depth estimate can be done by the measured pressure. Bottom track information is used to calculate the motion of the instrument when the frequency pulses reach the bottom and are consequently reflected back to the LADCP. From the bottom tracking, absolute velocities are found. Close to the ocean's surface, the VMADCP is used to constrain the velocities, and near the middle of the cast the GPS data improves the data quality by providing an estimate of the ship drift during the cast.

During this work, the processing software used to produce the LADCP products

was the LDEO. The code was originally written by Martin Visbeck (GEOMAR Helmholtz Centre for Ocean Research Kiel). In 2004 the user interface was re-designed by Andreas Thurnherr (Lamont–Doherty Earth Observatory - Columbia University). Currently, the software is maintained by the last.

Appendix C

Vertical Sections

C.1 Vessel-Mounted Acoustic Doppler Current Profiler (VMADCP) Velocities

The following figures (Figures C1 to C13) represent a linear interpolation of the meridional velocity profiles recorded by the VMADCP. The VMDCP data used during the BC analysis (section 3.1). The vertical sections that are represented on the figures correspond to sections S1 to S13 on Figure 3.3.

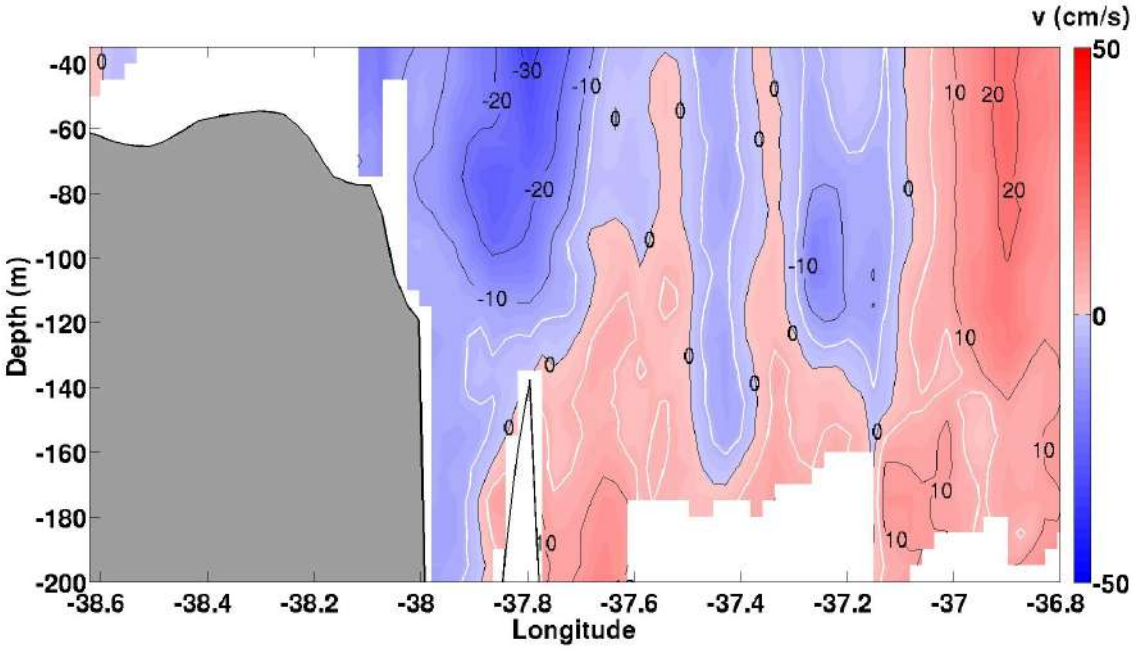

Figure C.1: Vertical section of the meridional velocity component in S1 (Figure 3.3).

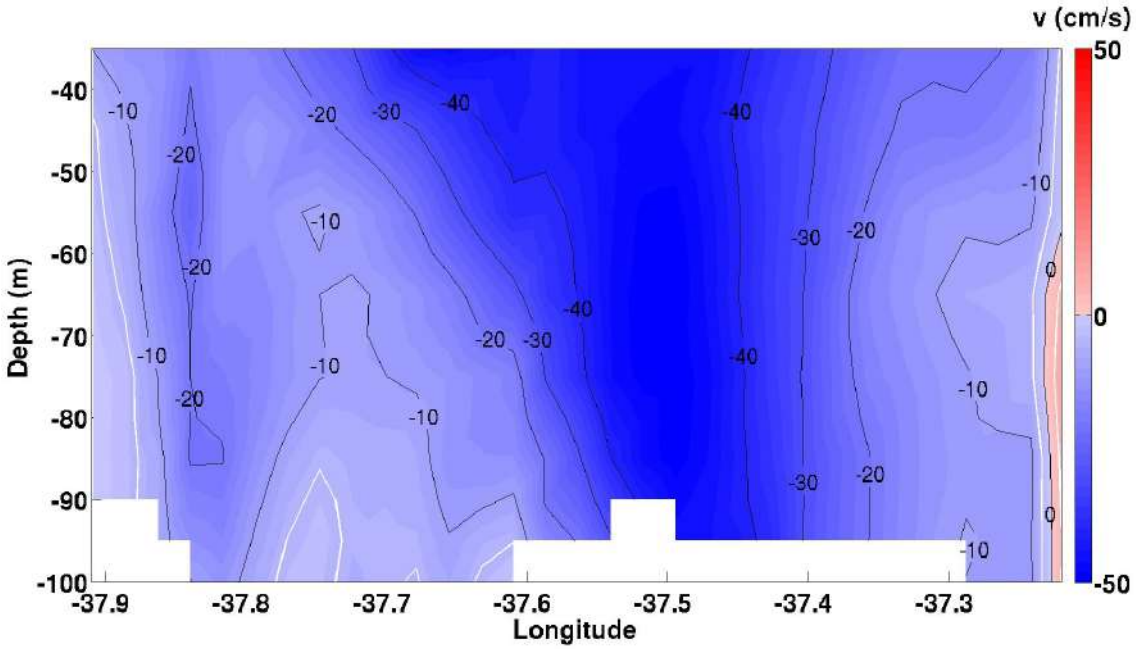

Figure C.2: Vertical section of the meridional velocity component in S2 (Figure 3.3).

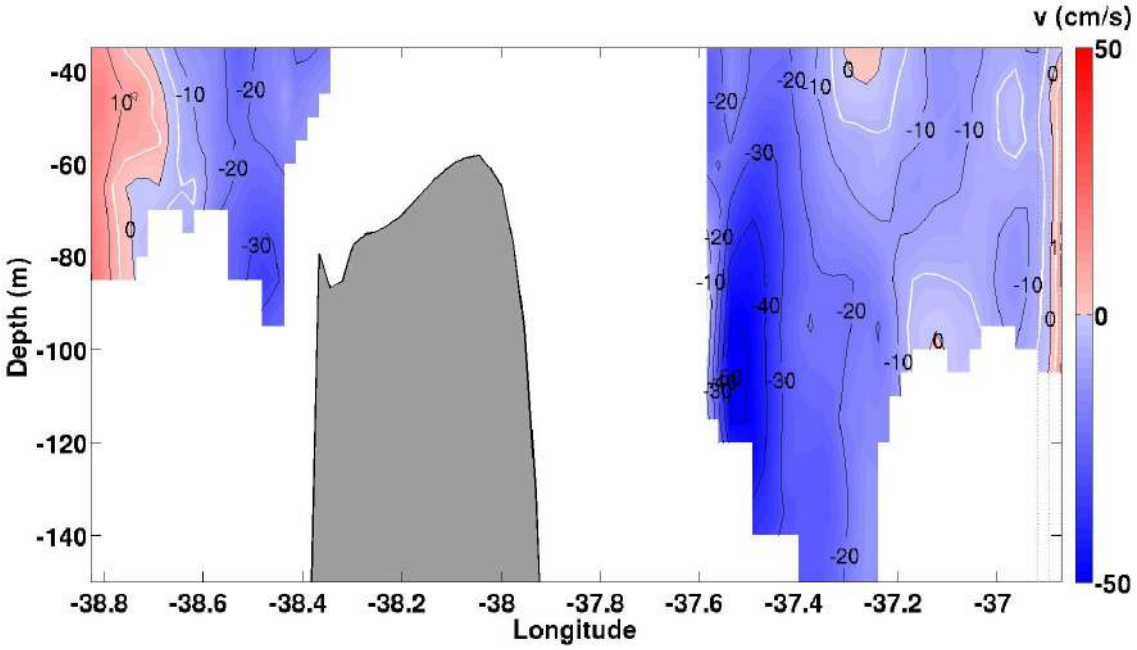

Figure C.3: Vertical section of the meridional velocity component in S3 (Figure 3.3).

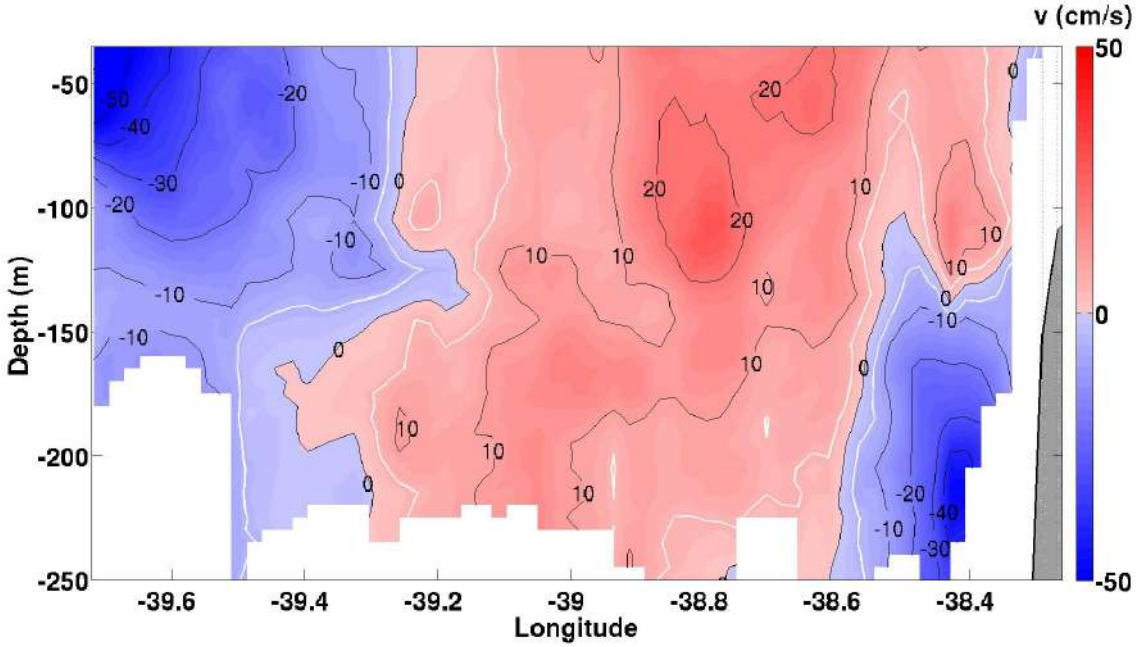

Figure C.4: Vertical section of the meridional velocity component in S4 (Figure 3.3).

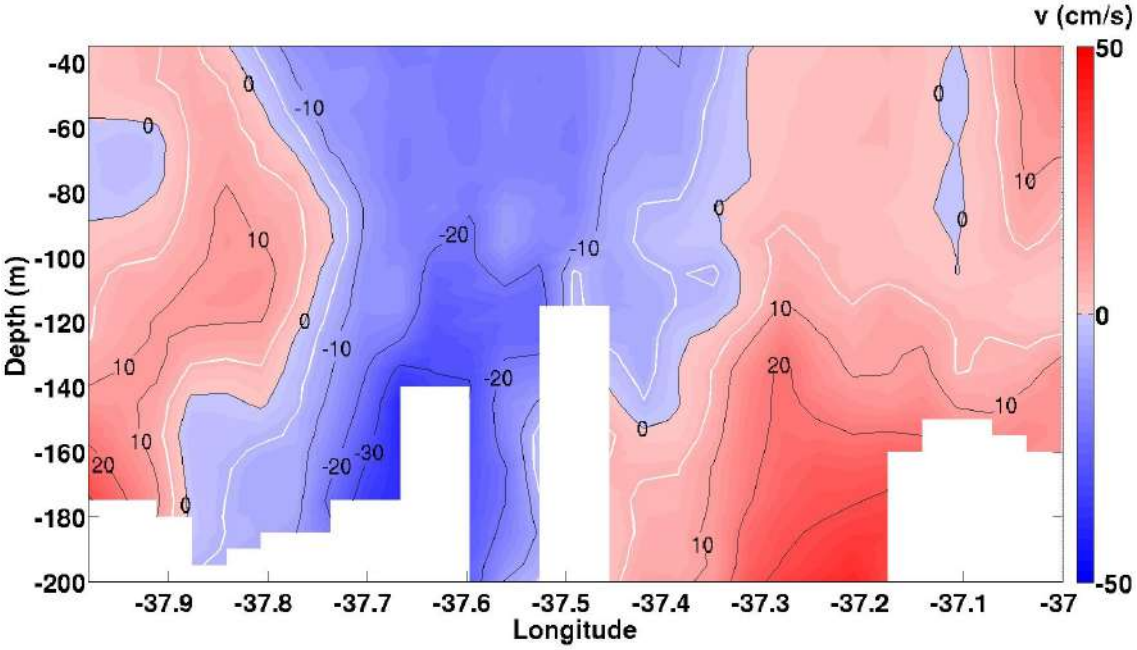

Figure C.5: Vertical section of the meridional velocity component in S5 (Figure 3.3).

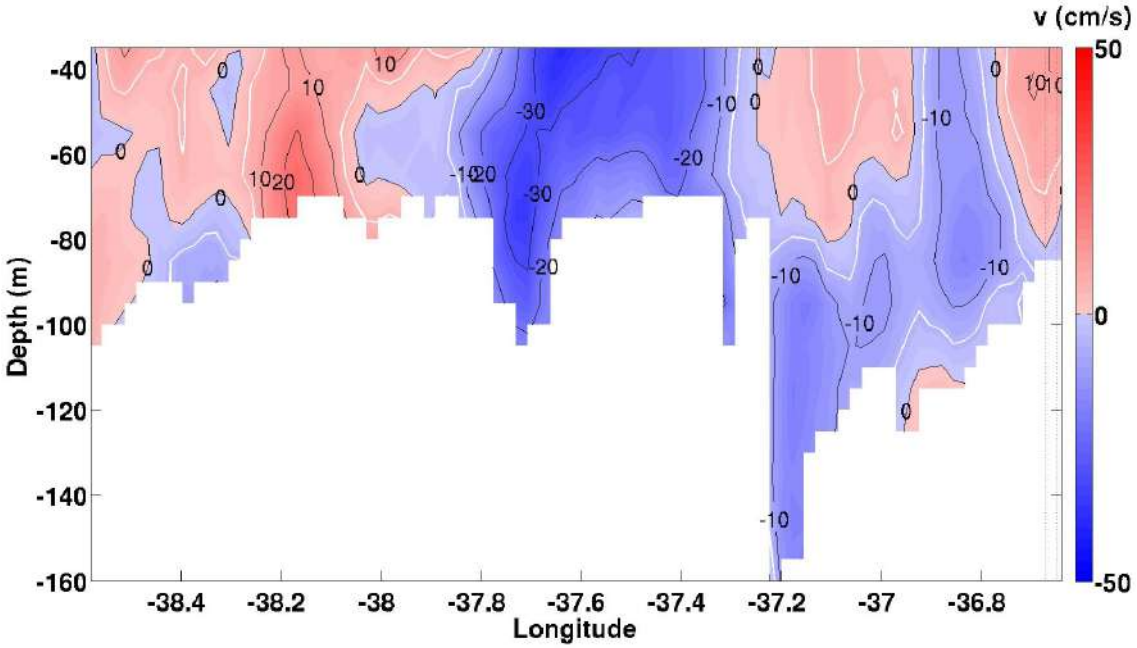

Figure C.6: Vertical section of the meridional velocity component in S6 (Figure 3.3).

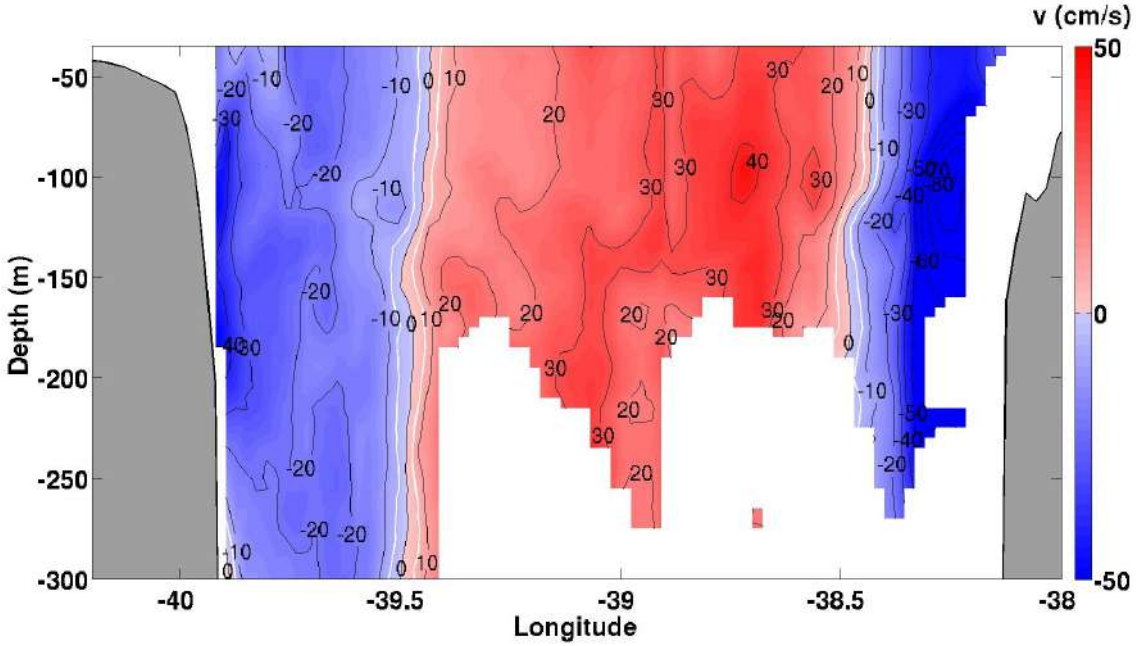

Figure C.7: Vertical section of the meridional velocity component in S7 (Figure 3.3).

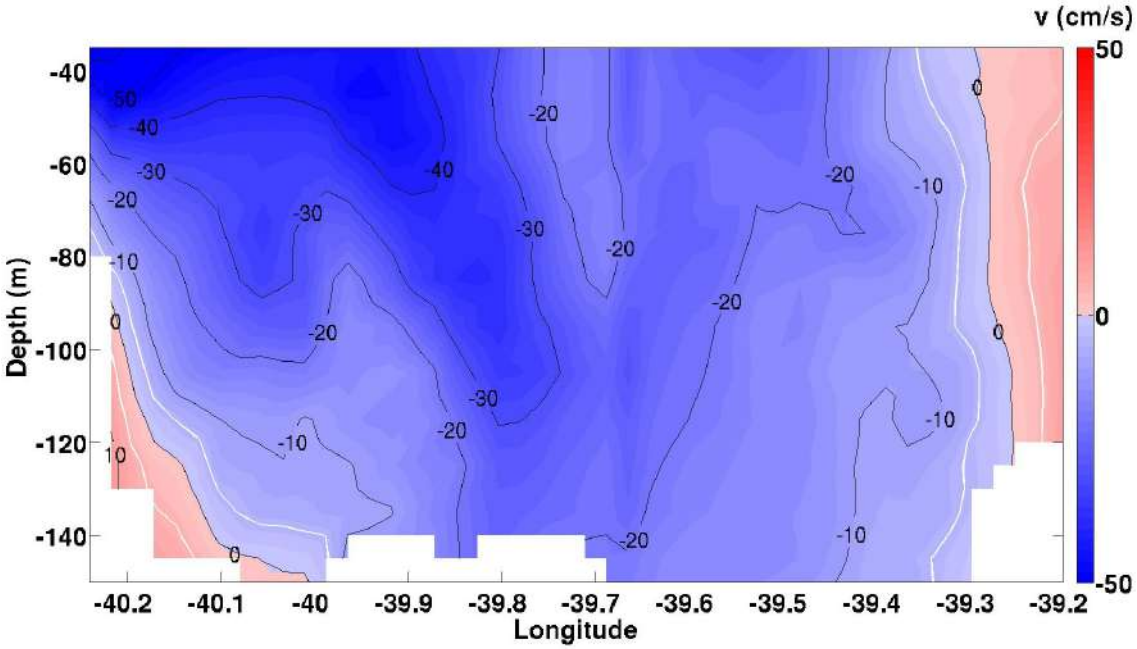

Figure C.8: Vertical section of the meridional velocity component in S8 (Figure 3.3).

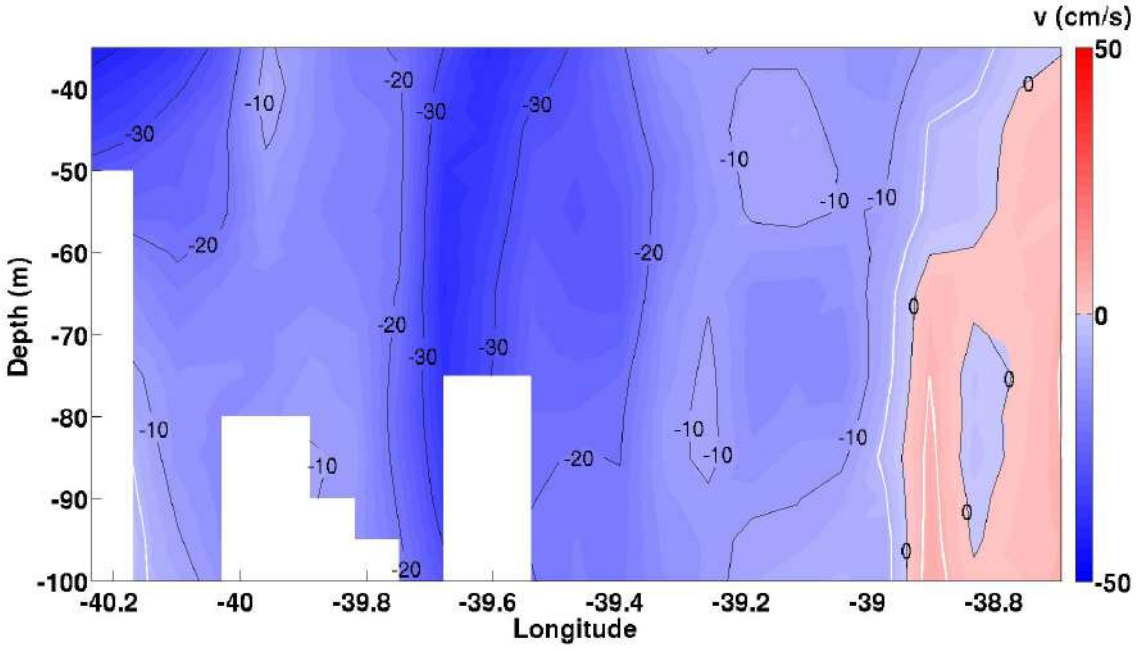

Figure C.9: Vertical section of the meridional velocity component in S9 (Figure 3.3).

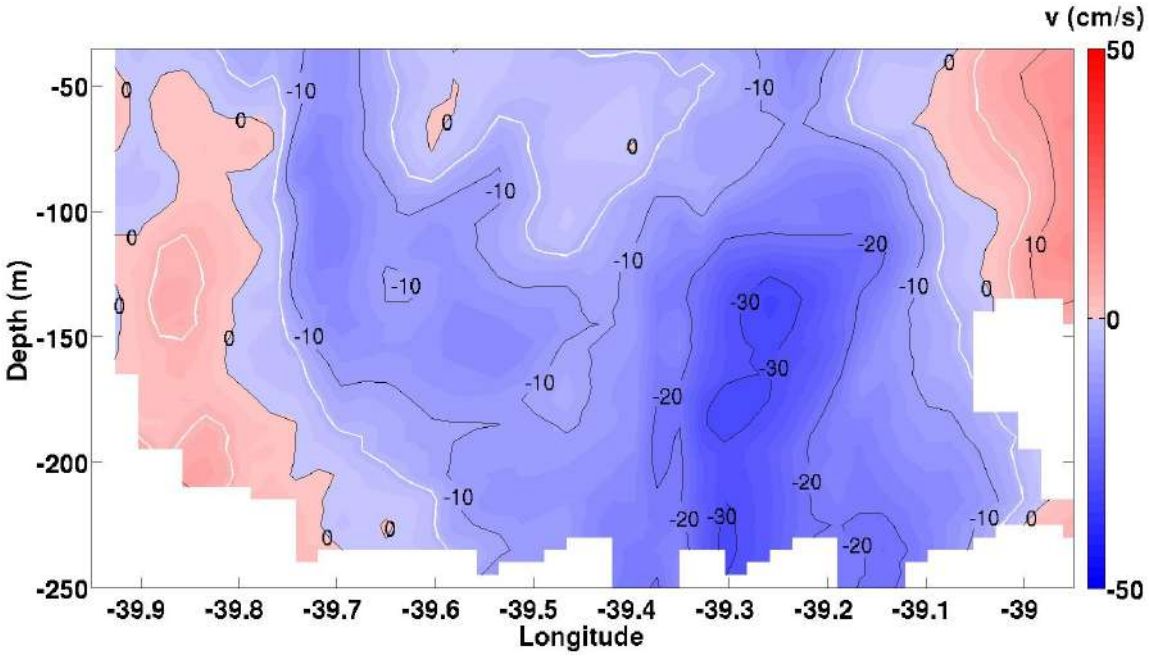

Figure C.10: Vertical section of the meridional velocity component in S10 (Figure 3.3).

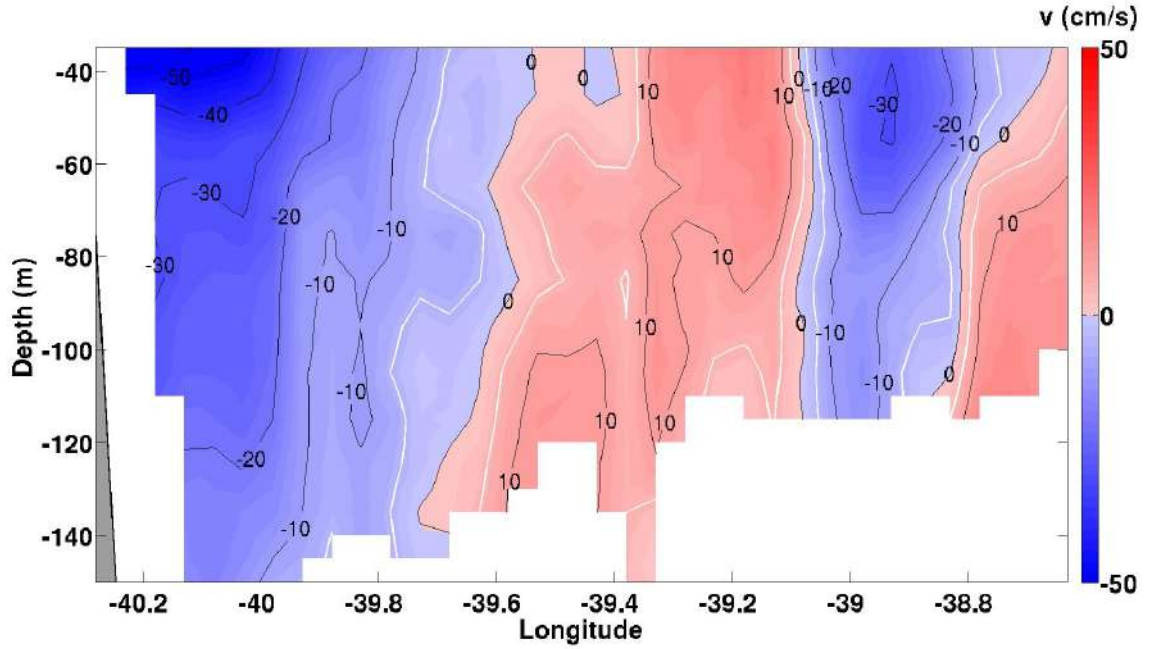

Figure C.11: Vertical section of the meridional velocity component in S11 (Figure 3.3).

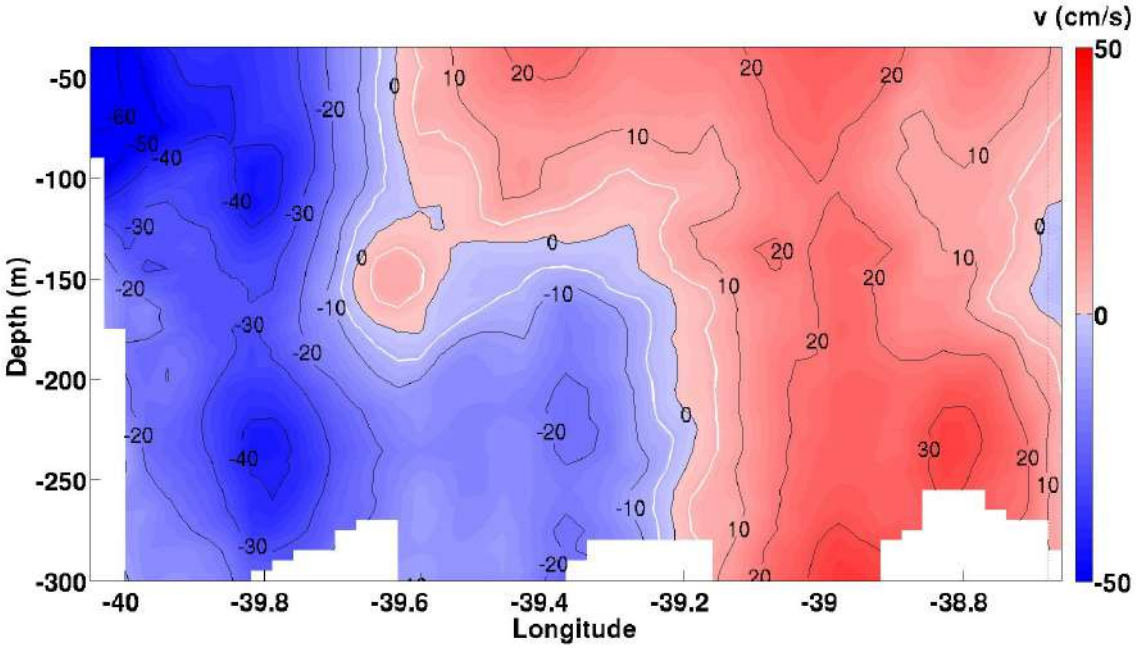

Figure C.12: Vertical section of the meridional velocity component in S12 (Figure 3.3).

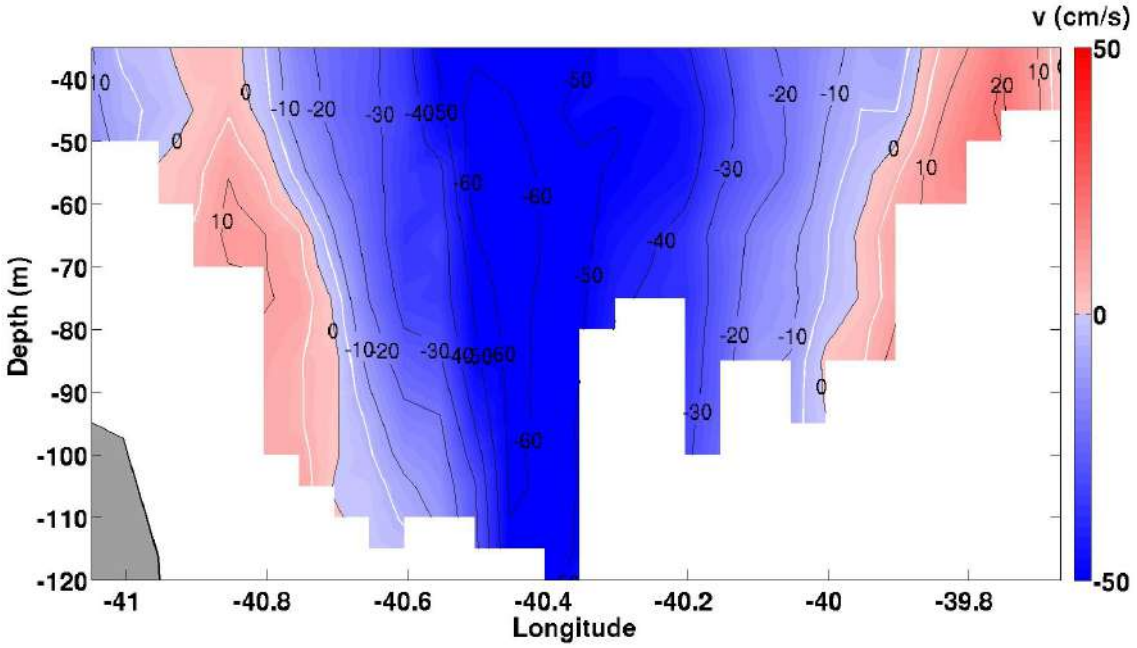

Figure C.13: Vertical section of the meridional velocity component in S13 (Figure 3.3).

C.2 Lowered Acoustic Doppler Current Profiler (LADCP) and Geostrophic Velocities

The following figures (Figures C14 to C22) represent a linear interpolation of the velocity profiles recorded by the LADCP or obtained geostrophically from CTD profiles. These data were used during the IWBC analysis (section 3.2). The vertical sections that are represented on the figures (Figures C14 to C22) correspond to sections C1 to C9 and C12 on Figure 3.4.

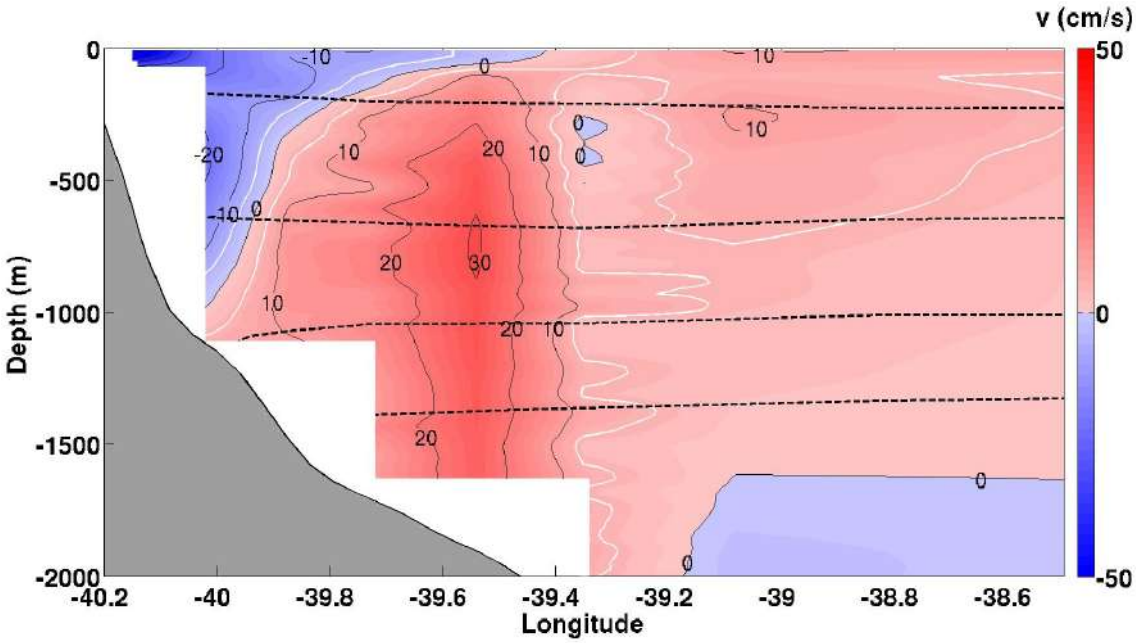

Figure C.14: Vertical section of the geostrophic meridional velocity component in C1 (Figure 3.4). From top to bottom, the dashed lines represent the potential densities of $\sigma_\theta = 26$, $\sigma_\theta = 27.05$, $\sigma_1=32$, and $\sigma_1=32.2$. The isopycnals limit the Tropical Water ($\sigma_\theta < 26$), SACW ($26< \sigma_\theta <27.05$), AAIW ($27.05< \sigma_0$ and $\sigma_1<32$), and Upper Circumpolar Water (UCPW - $32<\sigma_1<32.2$).

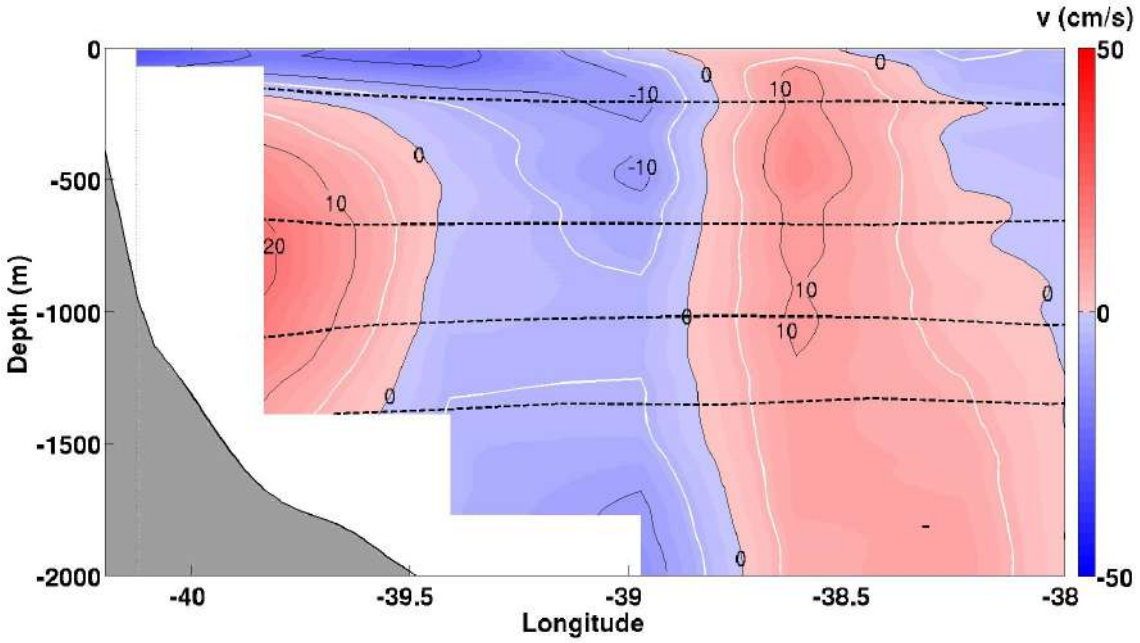

Figure C.15: Vertical section of the geostrophic meridional velocity component in C2 and C3 (Figure 3.4). From top to bottom, the dashed lines represent the potential densities of $\sigma_\theta = 26$, $\sigma_\theta = 27.05$, $\sigma_1=32$, and $\sigma_1=32.2$. The isopycnals limit the Tropical Water ($\sigma_\theta < 26$), SACW ($26< \sigma_\theta <27.05$), AAIW ($27.05< \sigma_0$ and $\sigma_1<32$), and Upper Circumpolar Water (UCPW - $32<\sigma_1<32.2$).

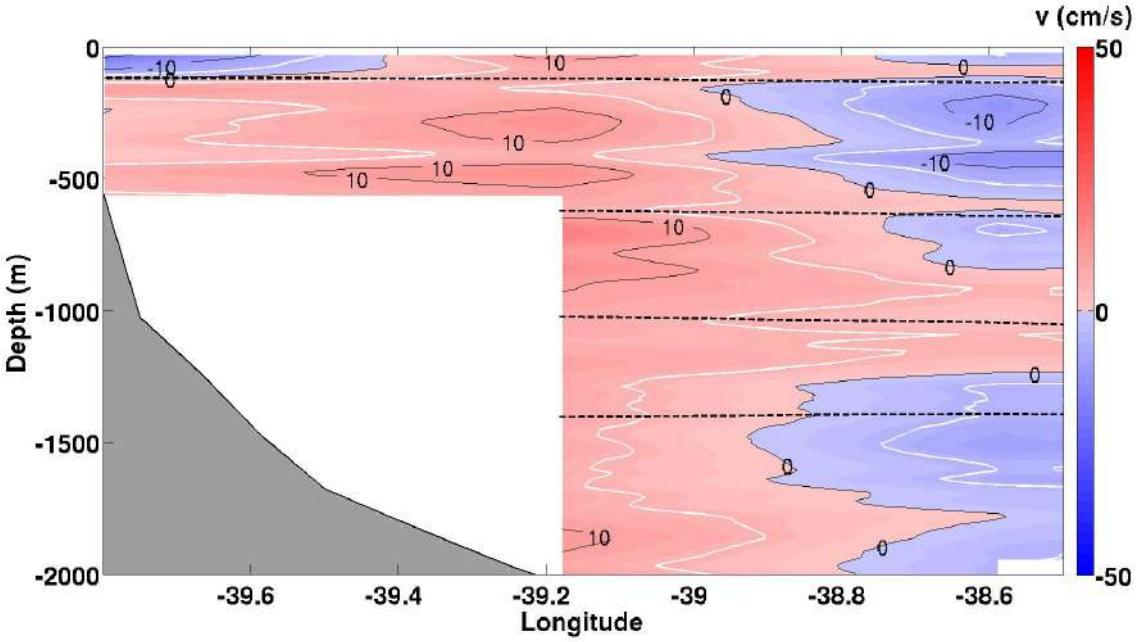

Figure C.16: Vertical section of the LADCP meridional velocity component in C4 (Figure 3.4). From top to bottom, the dashed lines represent the potential densities of $\sigma_\theta = 26$, $\sigma_\theta = 27.05$, $\sigma_1=32$, and $\sigma_1=32.2$. The isopycnals limit the Tropical Water ($\sigma_\theta < 26$), SACW ($26< \sigma_\theta <27.05$), AAIW ($27.05< \sigma_0$ and $\sigma_1<32$), and Upper Circumpolar Water (UCPW - $32<\sigma_1<32.2$).

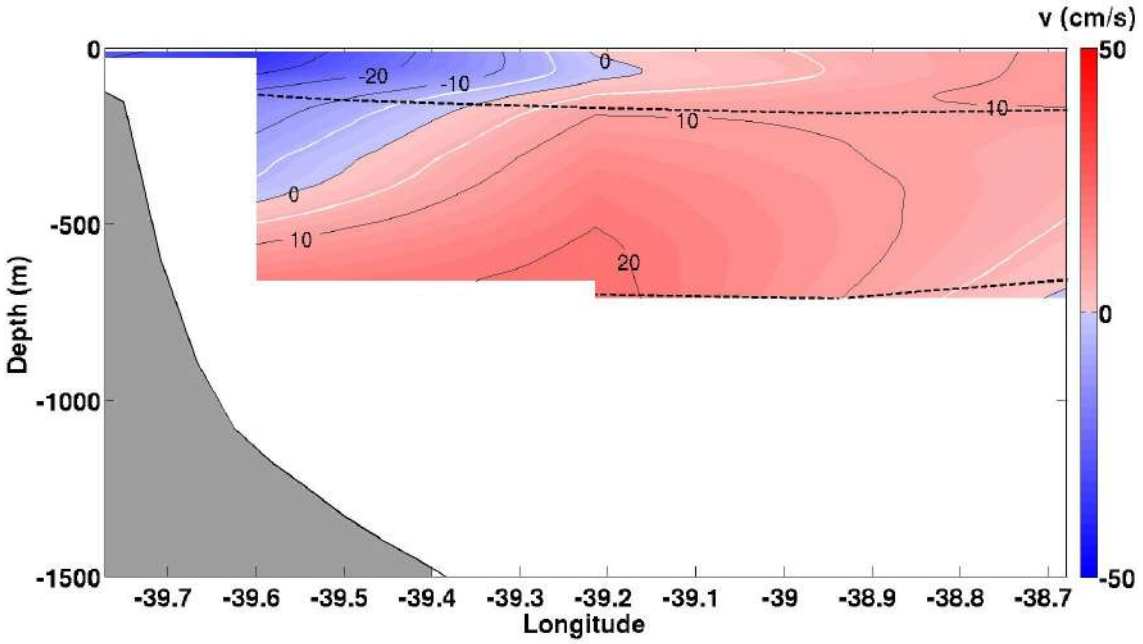

Figure C.17: Vertical section of the geostrophic meridional velocity component in C5 (Figure 3.4). From top to bottom, the dashed lines represent the potential densities of $\sigma_\theta = 26$ and $\sigma_\theta = 27.05$. The isopycnals limit the Tropical Water ($\sigma_\theta < 26$), SACW ($26 < \sigma_\theta < 27.05$).

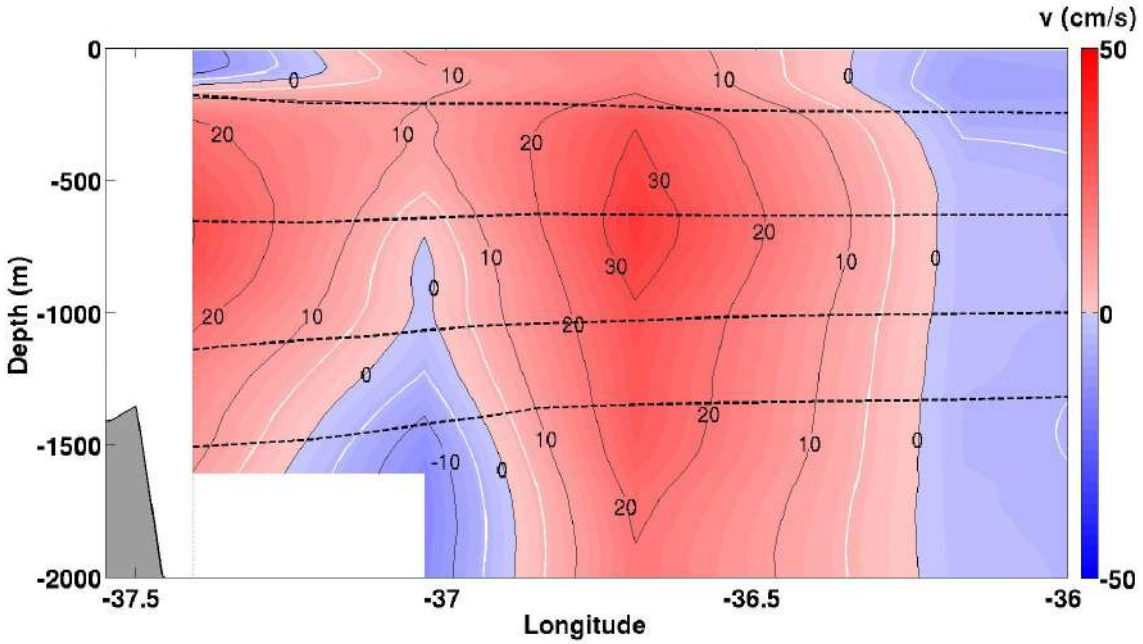

Figure C.18: Vertical section of the geostrophic meridional velocity component in C6 (Figure 3.4). From top to bottom, the dashed lines represent the potential densities of $\sigma_\theta = 26$, $\sigma_\theta = 27.05$, $\sigma_1 = 32$, and $\sigma_1 = 32.2$. The isopycnals limit the Tropical Water ($\sigma_\theta < 26$), SACW ($26 < \sigma_\theta < 27.05$), AAIW ($27.05 < \sigma_0$ and $\sigma_1 < 32$), and Upper Circumpolar Water (UCPW - $32 < \sigma_1 < 32.2$).

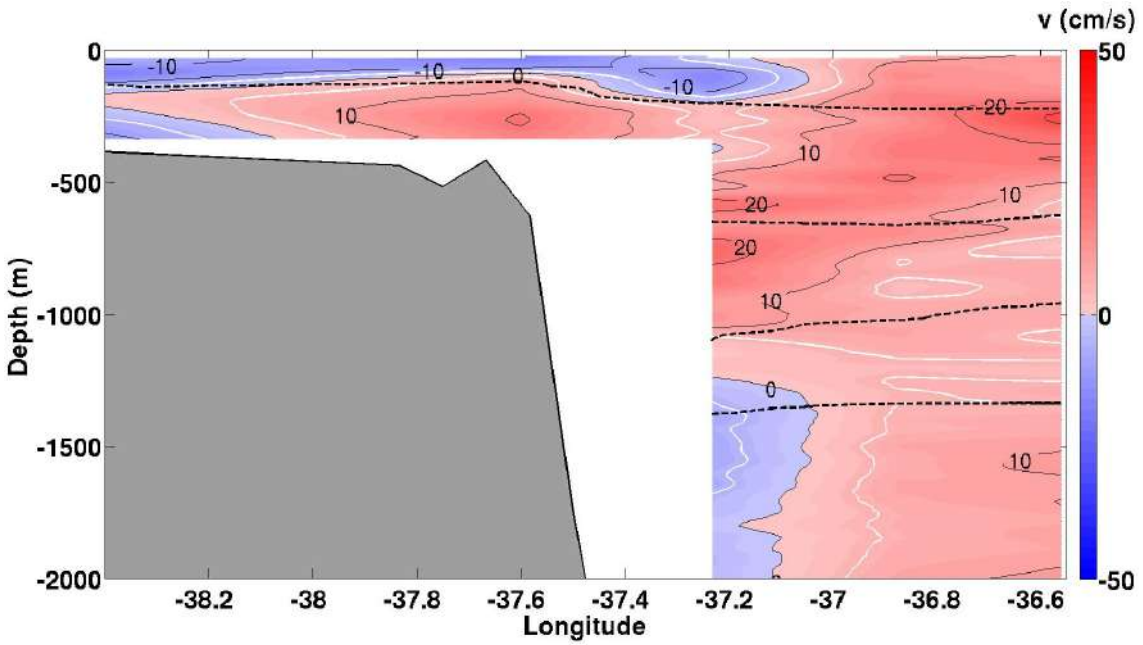

Figure C.19: Vertical section of the LADCP meridional velocity component in C7 (Figure 3.4). From top to bottom, the dashed lines represent the potential densities of $\sigma_\theta = 26$, $\sigma_\theta = 27.05$, $\sigma_1=32$, and $\sigma_1=32.2$. The isopycnals limit the Tropical Water ($\sigma_\theta < 26$), SACW ($26< \sigma_\theta <27.05$), AAIW ($27.05< \sigma_0$ and $\sigma_1<32$), and Upper Circumpolar Water (UCPW - $32<\sigma_1<32.2$).

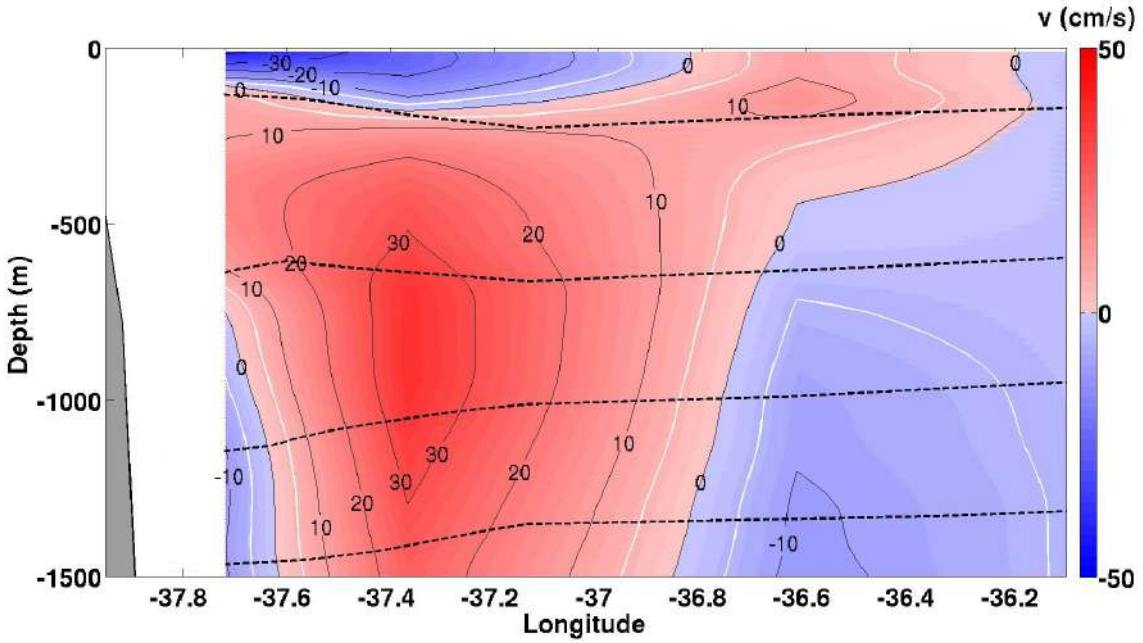

Figure C.20: Vertical section of the geostrophic meridional velocity component in C8 (Figure 3.4). From top to bottom, the dashed lines represent the potential densities of $\sigma_\theta = 26$, $\sigma_\theta = 27.05$, $\sigma_1=32$, and $\sigma_1=32.2$. The isopycnals limit the Tropical Water ($\sigma_\theta < 26$), SACW ($26< \sigma_\theta <27.05$), AAIW ($27.05< \sigma_0$ and $\sigma_1<32$), and Upper Circumpolar Water (UCPW - $32<\sigma_1<32.2$).

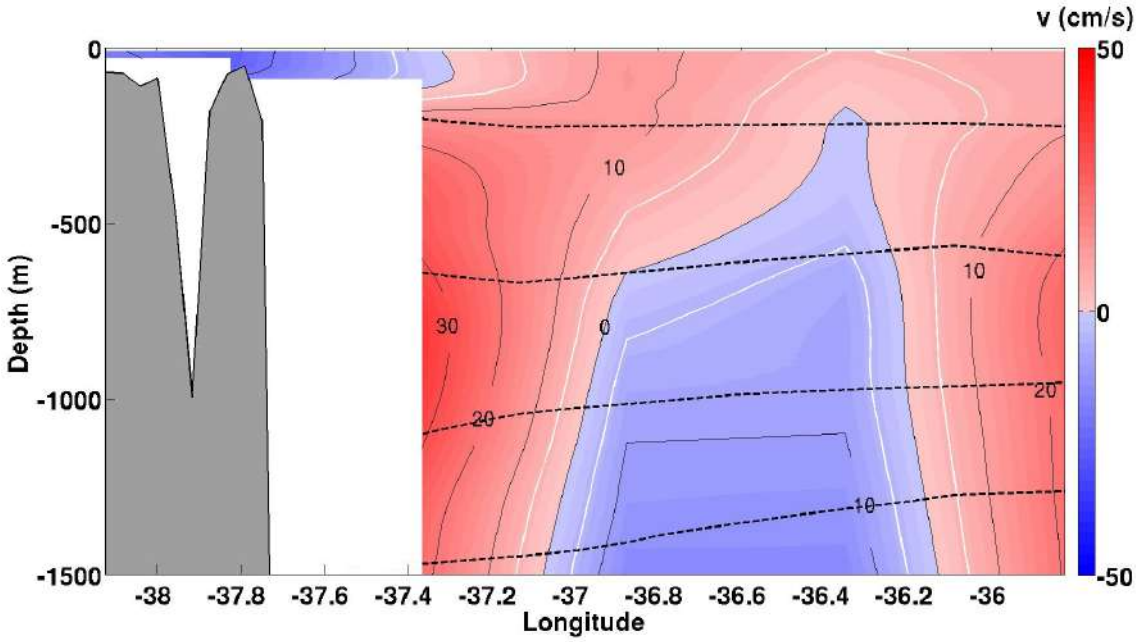

Figure C.21: Vertical section of the geostrophic meridional velocity component in C9 (Figure 3.4). From top to bottom, the dashed lines represent the potential densities of $\sigma_\theta = 26$, $\sigma_\theta = 27.05$, $\sigma_1=32$, and $\sigma_1=32.2$. The isopycnals limit the Tropical Water ($\sigma_\theta < 26$), SACW ($26< \sigma_\theta <27.05$), AAIW ($27.05< \sigma_0$ and $\sigma_1<32$), and Upper Circumpolar Water (UCPW - $32<\sigma_1<32.2$).

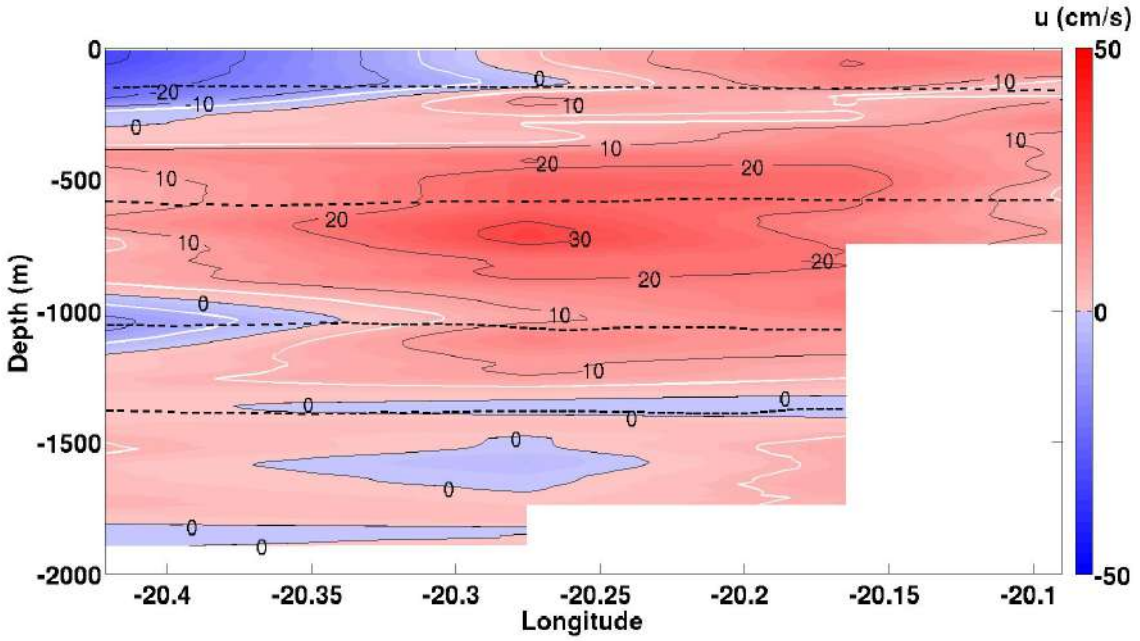

Figure C.22: Vertical section of the LADCP zonal velocity component in C12 (Figure 3.4). The axes were rotated 20 ° clockwise. From top to bottom, the dashed lines represent the potential densities of $\sigma_\theta = 26$, $\sigma_\theta = 27.05$, $\sigma_1=32$, and $\sigma_1=32.2$. The isopycnals limit the Tropical Water ($\sigma_\theta < 26$), SACW ($26< \sigma_\theta <27.05$), AAIW ($27.05< \sigma_0$ and $\sigma_1<32$), and Upper Circumpolar Water (UCPW - $32<\sigma_1<32.2$).